Evaluation of a Strut-Plasma Torch Combination as a Supersonic Igniter-Flameholder

Joseph Alexander Mozingo

Thesis submitted to the faculty of the Virginia Polytechnic Institute and State University
in partial fulfillment of the requirements for the degree of

Master of Science

in

Mechanical Engineering

Dr. Walter O'Brien
Dr. Joseph Schetz
Dr. Uri Vandsburger

February 23, 2004
Blacksburg, Virginia

Keywords: Plasma Torch, Strut, Supersonic Combustion

Evaluation of a Strut-Plasma Torch Combination as a Supersonic Igniter-Flameholder

Joseph Alexander Mozingo

Abstract

As the flight speeds of aircraft are increased above Mach 5, efficient methods of propulsion are needed. Scramjets may be a solution to this problem. Supersonic combustion is one of the main challenges involved in the operation of a Scramjet engine. In general, both an igniter and a flameholder are needed to achieve and maintain supersonic combustion.

The current work examines a plasma torch-strut combination as an igniter-flameholder. The plasma torch-strut combination was tested in the Virginia Tech unheated supersonic wind tunnel at Mach 2.4. Pressure and temperature sampling, filtered photography, and spectroscopic measurements were used to compare different test cases. These results provide both qualitative and quantitative results on how the combination responds to changes in the mass flow rate of fuel and the power to the plasma torch.

The key conclusions of the work were the following:
1. Tests showed that an exothermic reaction takes place.
2. The amount of heat release increases with an increase in the mass flow rate of fuel.
3. The plasma torch-fuel injector interaction caused the heat release to be well above the tunnel floor and sometimes off the strut centerline
4. One change in the fuel injector pattern caused more temperature rise near the floor of the tunnel.
5. The flow penetration height of the plasma torch alone was reduced by the fuel-plasma torch interaction.

6. Moving the strut upstream reduced the measured temperature rise at a fixed downstream location, but increased the penetration height of the plasma torch.

7. The computed heat release was found to be small compared to the potential heat release from all the fuel burning.

8. The amount of temperature rise caused by the fuel is not greatly affected by the power to the plasma torch.

Acknowledgements

Table of Contents

List of Figures

List of Tables

Chapter 1: Introduction, Background, and Motivation

The purpose of this study was to examine the performance of a strut-plasma torch combination as a supersonic flameholder and igniter. This work has application in supersonic combustion, and relates to the use of plasma torches as an igniter. The following sections give the background necessary to understand the importance of this work, and its relationship to other investigations with plasma torch igniters.

1.1 Supersonic Combustion

As the speeds of aircraft are increased to the Mach 5-8 range, traditional methods of propulsion, such as turbofan and turbojet engines, are not nearly as effective as they are at lower flight speeds. At these higher speeds, rocket engines have typically been used. Rocket engines have a major drawback in that not only the fuel, but also the oxidizer, must be carried onboard the aircraft. One way to eliminate this need is to use a supersonic combustion ramjet engine, which is known as a Scramjet. A Scramjet is an air-breathing engine, similar to a ramjet, which takes in air through an inlet and compresses the air. The air is compressed by diffusing the stream, and using the air's inlet momentum to increase the pressure. The difference between a ramjet and Scramjet engine is that the flow remains supersonic entering the combustor region of a Scramjet. Fuel is injected into this air stream in the combustor and ignited. The heated air is then accelerated through a nozzle to produce thrust. Scramjet engines have no moving parts in the main flow through the engine. This simple design and reduced flow losses makes Scramjets an attractive means of propulsion at high Mach numbers.

Scramjet research was started in the 1960s. However, the high temperatures caused by the deceleration of the high-speed flow at a Scramjet's operating speed,

combined with problems of sustaining efficient combustion have made the development of a Scramjet difficult. Recently, the materials available to engine designers have become more heat resistant. This increase in technology has led to a renewed interest in Scramjet research. Recent key programs have contributed much to the development of Scramjet engines. Probably the most important of these programs has been the research done on the National Aerospace Plane, which was started in the 1980s [Harsha et al., 1989]. The goal of this project was to design a vehicle that could take off and land like a conventional plane and deliver payloads to orbit. In order to be able to reach orbit economically, a Scramjet was to be used to accelerate the aircraft in the Mach 5-10 range. Because of funding problems, NASA ended the project in the mid 1990s.

Research in Scramjet engines was continued with programs such as the Hyper X, which is shown in Figure 1-1. The Hyper X program seeks to demonstrate the capability of Scramjet engines to power an aircraft in flight. Numerous tests have been done with the Scramjet engine in wind tunnels with good results [Northam et al., 1986]. Fundamental studies of supersonic combustion have also been done. The first model of the Hyper X, also know as the X-43A, seeks to demonstrate the possibility of accelerating an aircraft from Mach 5 to Mach 7 or 8 using a hydrogen fueled Scramjet. The X-43A is powered to a speed of Mach 5 by a rocket booster, and then separates from the booster. The Scramjet engine is then started to accelerate the aircraft. The first flight test of the X-43A was conducted on June 2, 2001. During the test the aircraft did not separate from its rocket booster and was lost. Because of the difficulties, no flight data could be gathered from the Scramjet engine. The next flight test is planned for early 2004.

Figure 1-1: The Hyper X concept aircraft that uses a Scramjet engine.

The next planned phase of the Hyper X program is the design and construction of a larger prototype, the X-43B. The X-43B will use both a turbojet and hydrogen fueled Scramjet engine to power the aircraft. The plane will take off from land, accelerate to around Mach 5 using the turbojet engine, and then switch to the Scramjet engine. The next plane in the program will be the X-43C, another small-scale airplane like the X-43A. The X-43C will seek to demonstrate the use of liquid hydrocarbon fuel in a Scramjet engine. The use of a liquid hydrocarbon fuel is an important step in supersonic combustion, as will be discussed later.

One of the most important areas of research in the development of Scramjet engines is supersonic combustion. In a supersonic flow, it is difficult to ignite and hold a flame. Fuel will autoignite in a Scramjet engine if the inlet Mach number to the engine is high enough, the conditions in the engine are right, and the geometry of the engine has been carefully designed. Autoignition occurs when the temperature rise resulting from the slowing of the inlet air is high enough that the fuel will burn as soon as it is injected into the flow. However, at relatively low flight speeds (around Mach 4), the air-fuel mixture in the engine will not autoignite. An igniter is needed to provide the energy necessary to ignite the air-fuel mixture at these relatively low speeds. Also an igniter may be needed if the flame in the engine is extinguished because of other circumstances, such as extreme maneuvers.

The high-speed flow through the engine not only makes it difficult to ignite the fuel, but also to keep the flame established in the combustor. The flow through the engine tends to blow the flame out of the engine. In general, some type of flameholder is needed to anchor the flame in the combustor. Typically these flameholders provide a region of slow or recirculating flow where combustion can be established. This region of combustion will then provide the energy necessary to continuously ignite the rest of the flow through the engine. This region is also where the fuel and air can mix together effectively. The fuel must be mixed both vertically out into the flow and laterally across the flow path. Flameholders achieve this mixing by incorporating the fuel injection in a manner that optimizes mixing.

In most Scramjet engines, both a flameholder and an igniter are needed. In the past, these parts were often designed as separate systems. However, as has been shown by Kimura et al. [1981] and Gallimore et al., [2001] the best performance from these devices can be achieved when the igniter and flameholder are designed to work together.

Traditionally, to reduce the difficulty of igniting and holding a flame in Scramjet engines, hydrogen was used as the fuel. Because hydrogen burns in air with a very high flame speed, it is able to burn during the short residence time of the combustor. The problem with using hydrogen is that it has a low energy density. Also, the fuel is difficult to store since it must either be at high pressure or low temperature to maximize the density of the fuel.

Recently for some Scramjet missions, the choice of fuel has shifted away from hydrogen to higher molecular mass hydrocarbons. These fuels provide a high heating value and a much higher density. They are also much easier to store. However, heavier hydrocarbons and liquid fuels are more difficult to burn because of their more complex composition and the need to atomize the fuel. These fuels react more slowly, are harder to ignite, and demonstrate a narrow range of equivalence ratios for combustion. This difficulty leads to the need for a more efficient flameholder and igniter.

In the past, several different types of flameholders have been used in supersonic combustion. Flameholders are designed so that they keep losses in the flow to a minimum, and are effective in anchoring the flame. The types of flameholders and their qualities will be discussed more in the next chapter.

1.2 Plasma Torches

A plasma torch is a device that creates a plasma from a feedstock gas that passes over an electric arc. Figure 1-2 shows a simplified diagram of a plasma torch. In a plasma torch, an arc is struck between the negatively charged cathode and the positively charged anode. A feedstock gas, such as nitrogen or a hydrocarbon like ethylene, is then

passed over the arc. Plasma torches have been used successfully as an igniter for many different combustion applications, which will be discussed in the next chapter.
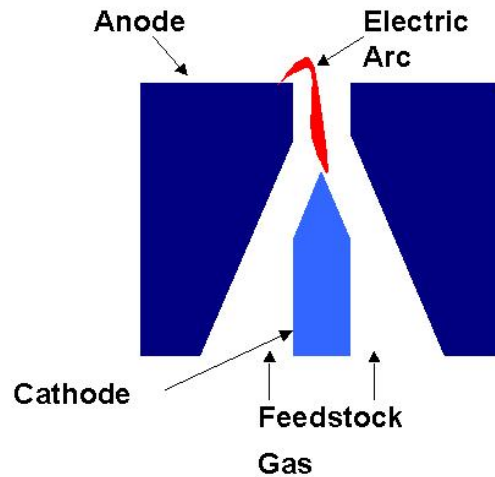
Figure 1-2: Schematic of the plasma torch concept.

The design of plasma torches presents several challenges to a designer. To strike an arc as is shown in Figure 1-2, the electrodes of the torch must be designed such that the preferred pat h for the arc is through the constrictor, which is the narrow, straight section of the anode. The internal geometry of the anode and the geometry of the cathode are the keys to controlling arc behavior.

Another design challenge is the material selection for the electrodes. The material must be able to withstand the extremely high temperatures over a small area caused by the attachment of the arc. Therefore, the material must have a high melting point and high thermal conductivity. The material must also be a good electrical conductor to be able to pass the current through without generating too much heat. Finally, the material must be relatively easy to machine. Because of the simpler geometry of the cathode, ease of machining is of less concern for the material used to make the cathode than for the anode. The material selection for the anode requires a compromise to reach the best combination of the three criteria described above. Copper, tungsten, and molybdenum are materials commonly used to make plasma torch electrodes.

Even the toughest electrode material available cannot continuously withstand the high temperatures produced at the attachment point of the arc. Therefore, some method of moving the arc attachment point is required. Two methods are currently used to

accomplish the movement of the arc. The first method is to use a magnet that has its poles aligned with the axis of the torch. The magnetic field generated produces a tangential force on any radial component of the arc. This tangential force will then spin the arc attachment point around the surface of the anode. The other method commonly used is to introduce a swirl to the feedstock flow. The swirling motion of the feedstock gas moves the attachment point of the arc on the electrode. The swirling of the flow also has other advantages that will be discussed in greater detail in the next chapter.

Another important aspect of torch design is the ability to be able to vary the power input to the torch. Varying the power allows the effect of the amount of plasma to be studied. The power used by a plasma torch, like all electrical systems, is related to the current and voltage. Typically the current can be controlled by the power supply of the torch and controls the diameter of the arc. The voltage is controlled by the length of the arc. Because the arc length is determined by the electrode gap, plasma torches typically have an electrode gap adjustment. Typical torch powers for combustion applications are in the 1 to 5 kW range.

The plasma created by a plasma torch has two attributes that make it effective in ignition. The first attribute of the plasma is that it is a source of thermal energy. As the gas flows over and through the electric arc, all of the gas is heated to some degree. This thermal energy is then used to help ignite the fuel-air mixture. In this sense, a plasma torch works much like a spark igniter or any other igniter. However, this is only one of the benefits of a plasma torch.

The second and perhaps most important attribute of the plasma is that it is a source of radicals that have the possibility of increasing the rate of combustion. A small amount of the feedstock gas passes through and close to the arc, which heats the gas to extremely high temperatures, over 3000 K. The high temperature of this small amount of feedstock causes the feedstock to disassociate producing radicals, which can enhance combustion. Combustion-enhancing radicals help to increase the rate of reaction of the fuel with the air by artificially increasing the concentration of certain radicals. This increase in the rate of reaction helps decrease the size needed for the combustor of the engine or increase the maximum flow that can be successfully burned in a given sized combustor.

The type of feedstock used determines whether the radicals produced will enhance combustion. The radicals produced should participate in the combustion of the fuel and last a long time before recombining. These criteria help to determine the feedstock that will be used. The power to the plasma torch determines the amount of flow heating and radicals produced. Higher powers also produce a larger diameter arc that will come into contact with more of the feedstock.

1.3 Motivation and Goals of this Study

The work presented in this study builds on and extends the work done in a previous study at Virginia Tech. In the previous study, an effective plasma torch was developed [Gallimore, 2001]. This torch was used in conjunction with an aeroramp injector block to study flameholding in a supersonic environment [Jacobsen, 2001]. An aeroramp is an array of injectors that enhances mixing and has an effect on the flow similar to a solid ramp, which is a common type of flameholder used in supersonic flow. For these experiments, ethylene was injected through the aeroramp injectors, and a number of feedstocks were used in the plasma torch. Because the wind tunnel used for both that study and the present study was unheated, the static temperature of the flow was on the order of 150 K. This low static temperature makes it difficult to ignite the fuel. Although it was not able to produce a robust flame, the aeroramp-plasma torch combination produced a plume that resulted from the cracking of the fuel, or breaking down into lower molecular weight hydrocarbons.

The purpose of the current research was to study the effectiveness of a strut-plasma torch combination as an igniter-flameholder in the same cold flow environment used in the previous aeroramp-plasma torch study. Ethylene was again used as the fuel, because it is a heavier hydrocarbon that is more difficult to burn than hydrogen, and has combustion properties similar to cracked liquid fuels. The properties of ethylene are representative of a heavier hydrocarbon and are given in Table 1-1. The laminar-premixed flame speed is shown for ethylene, while the current testing will be done with a

nonpremixed-turbulent flame. Turbulent flames can have a flame speed ten to twenty times higher than laminar flames, depending on turbulence levels and length scales. However, even the turbulent flame speed will be much less than the flow speed, which is on the order of 500m/s. Clearly a flameholding device is needed for ethylene combustion in a supersonic flow.

Table 1-1: Properties of Ethylene

Chemical Formula	Stoichiometric Air-Fuel Ratio	Higher Heating Value	Lower Heating Values	Adiabatic Flame Temperature	Laminar Flame Speed (at 1atm and Stoichiometric mixture)
C_2H_4	9.52	50,313 kJ/kg	47,161 kJ/kg	2,369 K	~0.7 m/s

A strut flameholder is often used in supersonic combustion applications because of its effectiveness. Although this effectiveness comes at a price of higher total pressure losses in the flow and cooling problems, a strut produces a fuel injection means, and a region of reduced flow velocity for flameholding. Nitrogen was used as the only feedstock for the torch, because of its previously-shown effectiveness [Harrison, 1971] and the longer electrode life it allows.

The overall goal of this study is to study the effectiveness of the wedge-plasma torch combination as an igniter-flameholder combination. The specific goals deal with judging both quantitatively and qualitative how well this combination works. Some specific goals are as follows:

1) Determine if producing and sustaining a flame is possible in a cold flow environment.
2) Study the effect of changing the fuel delivery, both amount and distribution of fuel, on the reaction observed.
3) Study the effect of plasma torch power level on the amount of reaction and heat release.
4) Study the presence of excited species in the area of reaction both spectroscopically and by using filtered photography.

This work is expected to contribute to the fundamental studies of the use of a plasma torch in a combined igniter-flameholder   The lessons learned in developing the strut

8

plasma torch igniter should be beneficial to engine designers. Also, spectroscopic measurements will allow a more detailed understanding of the reaction that takes place.

The following chapters present the relevant literature, the experimental setup, results from the experiments, and finally, the conclusions that can be drawn.

Chapter 2: Review of Relevant Literature

This chapter reviews and summarizes the most important studies related to plasma torch ignition and strut flameholders in supersonic combustion. As was described in Chapter 1, the area of supersonic combustion has received much attention over the past thirty years. Therefore, only the most relevant or novel studies are highlighted. This section first presents the history of augmenting combustion with plasma torch. Discussed next is the development of strut flameholders. Finally, the motivation for the present study is discussed.

2.1 History of Plasma Torches in Supersonic Combustion

The first use of a plasma torch to augment combustion was reported in the 1960s. Lawton et al. [1962] and Chen et al. [1965] used a plasma torch to increase the flow rate through a burner. The goals of that study were to increase the specific energy output of a burner, and also to add ionized species to the products produced by this burner. The authors found that with the addition of a plasma torch to the burner, the flow rate through the burner could be increased by 350% over the flow rate without the plasma torch. The arc in the plasma torch used in that study was magnetically rotated. The authors believed that the plasma torch was most effective when the arc was rotated at very high speeds. It was thought that by rotating the arc at very high speeds the feedstock would be evenly heated coming out of the torch. The authors dismissed the use of a vortex to spin the arc because the arc would be in contact only with a small portion of the feedstock gas.

Harrison et al. [1971] continued the work of the Lawton and Chen. They studied the effects of varying the feedstock and the rate of rotation of the arc on the maximum flow rate through the burner. They found that using argon in the torch improved the

maximum flow rate through the burner by 300%. By using nitrogen instead of argon, the effectiveness of the torch was doubled to 600% over the baseline case. Air and oxygen were also tested as feedstocks, and they were found to have an effectiveness between that of argon and nitrogen. The authors expected oxygen and air to be more effective than nitrogen alone, because the oxygen radicals formed in the plasma are expected to participate directly in the combustion reaction.

The unexpected good result with nitrogen could be explained by the lifetime of the radicals produced. Oxygen radicals are extremely reactive and recombine very quickly. The nitrogen radicals produced are longer-lived. This longer life enables the nitrogen radicals to be just as effective as the oxygen radicals. The nitrogen radicals can then indirectly produce oxygen radicals by the reaction shown in equation 2-1:

$$N + O_2 \rightarrow NO + O \qquad\qquad (2\text{-}1),$$

The oxygen radicals can then participate directly in the combustion process. Using nitrogen as the feedstock also has an advantage in that nitrogen is less erosive to the electrodes than the oxygen feedstock.

Harrison, et al., also showed that the plasma torch was more effective than predicted by the analytical results adding the equivalent amount of heat provided by the torch to a perfectly stirred reactor. This result shows the importance of the species produced on the effectiveness of the torch. Because of the importance of species produced, the authors were the first to suggest that it might not be necessary to heat the feedstock evenly. They suggested that heating a smaller portion of the feedstock to a much higher temperature may be more beneficial than heating all of the feedstock evenly. The radicals produced were expected to live longer in a higher temperature environment. Therefore, having a small area of extremely hot feedstock could be more beneficial than trying to heat all of the feedstock evenly.

Weinberg et al. [1968] and Orrin et al. [1981] continued research into the use of plasma torches in combustion throughout the 1970s and 1980s. However, most of their research involved the use of pulsed plasma torches that would be used to replace a conventional spark plug in an internal combustion engine. Although this work has no direct application to supersonic combustion, it does deal with the development of plasma torches for combustion applications.

Two results by Weinberg and his associates are of particular note. The first result was that although some species are not as long-lived as nitrogen radicals, they can be just as effective. The radicals can be more effective if they have a higher diffusivity than nitrogen radicals. This higher diffusivity increases the rate at which the radicals are transported throughout the flow. Higher diffusivity is usually found in lighter molecules, such as hydrogen. The second important result found was that a plasma torch could be used to ignite a fuel air mixture that was well above the rich flammability limit. These rich mixtures were at equivalence ratios that would not be flammable if a conventional spark plug was used as the igniter.

Kimura et al. [1981] were the first to use a plasma torch in a supersonic combustion application. Following the experience of Weinberg in applying plasma torches to simple burners and to internal combustion engines, Kimura et al. tested a plasma torch for supersonic combustion augmentation. In order to be successful, Kimura reasoned that the plasma torch must be able to increase the reaction rate of the fuel with the air, while requiring a relatively small amount of energy, when compared with the overall chemical energy of the system.

Kimura et al. tested the plasma torch with a simple fuel injection system at various inlet Mach numbers and low static temperatures. Previous studies had shown that lowest static temperature at which combustion with hydrogen could be established was 700 K. With the use of a plasma torch, the authors produced combustion in a Mach 2.1 flow with a static temperature on the order of 150 K. Combustion was possible when the power added to the system by the plasma torch was as little as 2% of the overall chemical energy of the system. Increasing the inlet Mach number decreased the effectiveness of the plasma torch, but combustion was still possible.

The plasma torch was placed both upstream and downstream of the fuel injectors. If the plasma torch was placed upstream of the fuel injectors, some combustion of the fuel would take place. The plasma torch was found to be most effective when placed downstream of the fuel. However, if the plasma torch was placed too close to the fuel injection, no combustion was observed. The authors suggested that this finding was because the plasma torch only heated, but did not ignite, the fuel. These results

demonstrate that the placement of the plasma torch can be critical to the overall performance of the system.

In addition to varying the location of the plasma torch with respect to the fuel injectors, Kimura et al. also tested the torch with different feedstocks and powers. The authors found hydrogen and nitrogen to be equally effective in promoting combustion at the same net power. The net power is the power supplied by the arc to the feedstock. The rest of the power supplied to the arc goes into heating the electrodes and is lost to the cooling water. The power supplied to the plasma torch was measured and nitrogen was found to be more effective than hydrogen. The authors suggested that hydrogen loses some of its effectiveness due to the high heat loss caused by its high thermal diffusivity. Increasing the power improved the effectiveness of the plasma torch up to a power of 3 kW.

Warris et al. [1984] tested both a continuous and pulsed plasma torch in a relatively low speed flow. The tests were done in a 5 to 30 m/s flow, which is in the low subsonic region. The authors showed that it was possible to ignite a lean mixture of fuel and air when ignition would otherwise not be possible. The authors found that a nitrogen plasma was very effective in igniting the flow. The authors also showed that an argon plasma was not effective at all. Therefore, the energy added to the flow had a negligible effect on the ability of the plasma torch to produce a stable flame. The effectiveness of the plasma torch was due to the specific excited species produced by the torch.

Wagner [1987] investigated whether or not a plasma torch could be used as a replacement for silane. Silane is pyrophoric, which means that it will burn at room temperature when exposed to air. Silane is mixed with the fuel to cause ignition, but because silane is so reactive, it is difficult to store and transport. The goal of Wagner's study was to see if hydrogen radicals supplied by a plasma torch could be an effective replacement for silane.

Using the torch developed by Barbi [1986], Wagner was able to show that a plasma torch could be used as an effective replacement for silane. Wagner tested the plasma torch in a heated, supersonic wind tunnel. The plasma torch was placed behind a rearward-facing step with the hydrogen fuel injected both upstream and downstream of the torch. The plasma torch was most effective when operating on a 1:1 mixture of

13

hydrogen and argon at power levels as low as 630 W. Although the argon does not provide any combustion-enhancing radicals, its presence stabilized the arc. This feedstock proved to be the best compromise between supplying the most effective radicals to the flow, while maintaining stable operation of the torch. The effect of the plasma torch was to lower the tunnel total temperature at which ignition of the fuel was possible. The performance of the plasma torch was found to be equivalent to an addition of 20% silane to the fuel. Also, the plasma torch was able to reduce the inlet total temperature required to ignite the fuel from the autoignition temperature of 1470K to 890K, a reduction of over 33%. Only Wagner's supersonic combustion results will be discussed here. The torches used by Wagner are discussed in Appendix A.

Wagner also tested the plasma torch without the rearward-facing step [Northam, 1984]. Wagner found that the torch could operate as a both an igniter and flameholder by itself. The plasma torch performed best with fuel injected both upstream and downstream of the torch. Also, the flame produced would immediately extinguish when the plasma torch was turned off. This was seen as a promising result for the use of a plasma torch as both an igniter and flameholder.

Sato et al. [1992] tested a plasma torch that was developed to operate on a feedstock of nitrogen or air. The plasma torch was placed upstream of the fuel injectors. The plasma torch was located in the bottom wall of the rig, with fuel injectors located in both the top and bottom walls of the setup. A step flameholder was just downstream of the fuel injectors on the bottom wall. The fuel injection scheme, whether just the top or the top and bottom injectors were used, was varied to test the effectiveness of a single plasma torch as an igniter for supersonic combustion. The plasma torch was tested with a power of around 3 kW. The authors found that the plasma torch was effective igniting the fuel from the injectors on the bottom of the test cell, but could not ignite the fuel from the fuel injectors on the top. They also found that the plasma torch could be turned off and the flame would remain anchored in the test cell. Air and oxygen were found to be equally good as feedstocks for the plasma torch.

Masuya et al. [1993] studied the effect of plasma torch parameters on the total temperature at which the plasma torch would ignite the fuel. The plasma torch was placed on the bottom wall of the test section, upstream of the fuel injectors. A pilot fuel

14

injector was located on the top of the test section. The main flow of fuel came from the sides of the test section. Increasing the input power to the torch was found to linearly decrease the total temperature of the flow at which combustion could be established. The flow rates of the all feedstocks, except for oxygen, were found to have no effect on the ignition temperature. When using oxygen as the feedstock, increasing the flow rate decreased the ignition temperature. This increase in effectiveness was believed to be caused by the reactivity of oxygen radicals. The authors also found that the effectiveness of a mixture of argon and hydrogen was an effective feedstock when small amounts of hydrogen were added. After a small amount of hydrogen was added, around 5%, the effectiveness did not increase much. Therefore, the addition of a small amount of hydrogen seems to have a positive chemical effect. Also, the plasma torch was found to be effective for equivalence ratios below 0.4.

Takita et al. [2000] performed calculations as well as experiments on a plasma torch with different feedstocks operating in a supersonic cross flow. They found that monatomic N radicals were quickly converted to O radicals by the process shown in equation (2-1) above. N radicals were produced in the lowest power case, despite the fact that calculations based on thermochemical equilibrium showed no presence of radicals. This difference was likely due to the nonuniformity of the temperature distribution at the torch exit. This nonuniformity was caused by the arc heating the nitrogen closest to the arc and not heating all of the nitrogen evenly, which the calculations could not take in to account. The amount of radicals produced by the plasma torch was found to increase with increase in power for both O_2 and N_2 feedstocks. The regions of N or O downstream of the torch were found to be very small.

Gallimore [2001] tested an integrated igniter-flameholder system that used a plasma torch and an aeroramp injector. An aeroramp injector is an array of fuel injectors arranged in such a way as to present gas injected as an obstruction to the flow, as well enhancing mixing. This obstruction is meant to appear to the flow in much the same way as a physical ramp. Drawings of an aeroramp and a physical ramp are shown in Figure 2-1. This obstruction to the flow causes areas of recirculation, which are useful for flameholding.

<div align="center">(a)   (b)</div>
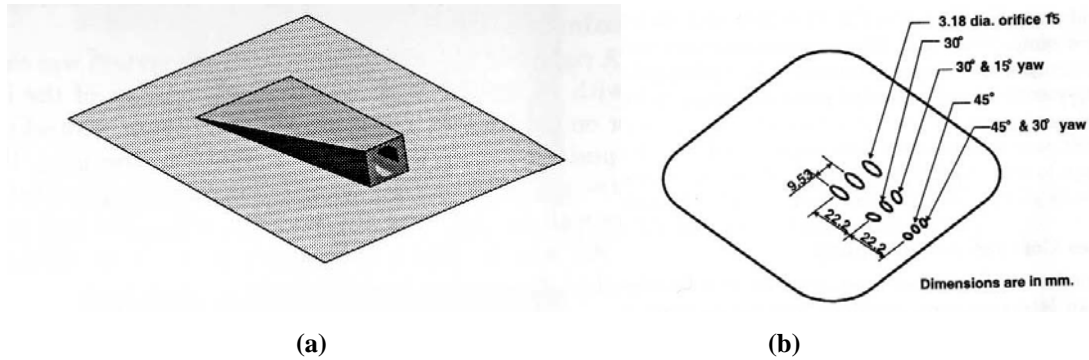
Figure 2-1: Comparison of (a) physical ramp and (b) aeroramp flameholders [Fuller et al. 1996]

Although Gallimore was never able to produce a flame in the unheated tunnel, he was able to produce a combustion plume thought to be due to pyrolysis of the fuel. Moreover, he found that the presence of the aeroramp greatly increased the penetration of the plasma plume into the flow. This increased penetration made the plasma torch more effective than it would have been alone. This increase in effectiveness shows that to achieve the best possible results, the plasma torch and injection scheme had to be designed to work together. If the placement and design of the torch and injectors were not correct, then the positive effects of the torch were not achieved.

2.2 Strut Flameholder Background

Strut flameholders have been used since the early development of ramjet engines. A strut offers a relatively large wake region in which to mix and burn the fuel. However, the strut causes large drag losses and can be troublesome to cool at high Mach numbers. Therefore, much of the recent research in flameholders has been with devices such as cavities or aeroramps, which produce the low-speed strong-mixing area needed for flameholding, with much lower drag losses.

In the present study a strut was chosen as a way to introduce fuel into the flow away from the wall of the wind tunnel, as well as to provide a wake region in which the

fuel would burn. Therefore, an extensive history of strut flameholders is not given in this section. Only results related to plasma torch applications will be discussed.

Masuya et al [1995] tested strut flameholders with a plasma torch placed on either side of the strut in the floor of the heated wind tunnel. Pilot hydrogen fuel was injected upstream of the plasma torch with the main hydrogen fuel injection coming from the sides of the strut just behind a step. The plasma torch operated at a power of 1 kW with either oxygen or air as the feedstock. They found that the most flow-disturbing strut was the most effective flameholder. Also, the author found that the plasma torch could ignite the main fuel injection flow as long as there was pilot fuel injected upstream of the plasma torch. This means that the radicals from the plasma torch could not exist for very long in the main flow of the wind tunnel. The authors also found that the more pilot fuel injected, the lower the total temperature required to achieve forced ignition with the plasma torch.

Brandstetter et al [2003] tested a strut flameholder with injection both perpendicular to the slanted surface of the strut and in the wake of the strut. The cross-flow could be heated to 700 K, and the flame was started with a pulsed laser beam. A cylindrical flame holder was needed downstream of the strut in order to maintain a flame. The cylindrical flameholder was heated during the time when the laser ignition system was on. The laser could then be switched off, while the hot surface of the flameholder sustained the combustion. The combustion near the flameholder kept the flameholder hot, producing a self-sustaining system.

Chapter 3: Experimental Setup

All testing for this study was done in the Virginia Tech supersonic wind tunnel using the Virginia Tech plasma torch. This chapter describes the equipment and procedures used the tests in this study. The test equipment, setup, and the measurement systems are described. Finally, the test procedures are discussed.

3.1 Test Equipment

The components used for all tests other than the measurement systems can be grouped into four categories. Each category will be described in this section. The categories that are discussed are the strut, plasma torch, flow system, and finally the supersonic wind tunnel.

3.1.1 Strut

The strut used in this study was not a design that would be used in a realistic Scramjet engine. The strut was originally designed for study of burning in a wake region, for use as a device for sonic boom reduction. More information about the sonic boom reduction work can be found in Marconi, [2001]. Even though this strut does not represent an optimum supersonic combustion strut, it remains a useful device to study how well a plasma torch can ignite fuel injected well above the plasma torch, in a wake region.

A drawing of the strut used is shown in Figure 3-1. The strut is 101 mm high, has a chord of 38.1mm and a thickness of 6.35mm. The size of the strut was determined by the test section size. The thickness of the strut was small compared to the test section to minimize disruption of the flow. All distance measurements in this study were non-dimensionalized by the strut thickness. Fuel injection was accomplished by drilling a hole vertically through the strut to make a plenum. Small holes were drilled in from the back of the wedge to serve as the actual fuel injectors. The fuel injection holes extend 32 mm up the back of the wedge. Originally, all of the fuel injection holes were the same diameter of 0.51 mm. Later, the bottom four holes were increased to 0.71 mm. This change will be explained when discussing the measured total temperature results.
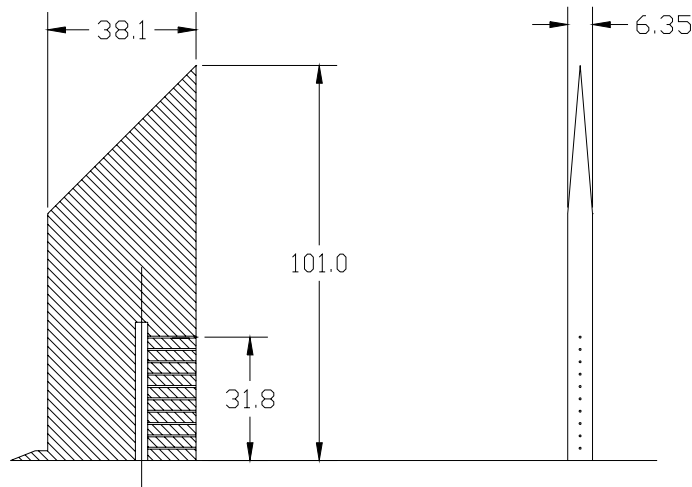
Figure 3-1: Schematic of strut used (all dimensions in millimeters)

3.1.2 Plasma Torch

The plasma torch used in the current work, shown in Figure 3-2, was developed by Gallimore [2001] and Jacobsen [2001]. This torch incorporated the most important features from the earlier Virginia Tech plasma torches as well as some new features to make the torch easier to assemble and to allow the torch to operate more stably. A brief history of the development of the Virginia Tech Plasma Torches is given in Appendix A. Operation of the torch was possible at power levels from 750 W to 4500 W. In the present study, the only feedstock used was nitrogen. Nitrogen, as explained in the

previous chapter, produces long-lived species that can participate, although indirectly, in the combustion process. Also, nitrogen was the least erosive feedstock tested by Gallimore.
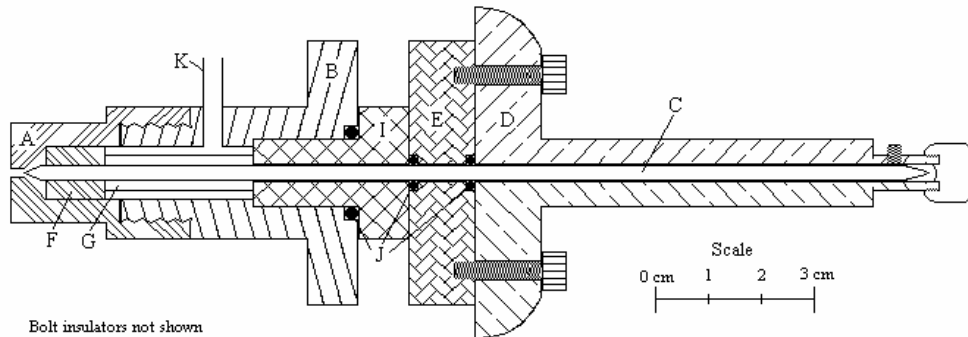
Figure 3-2: Section drawing of plasma torch used (adapted from Gallimore [2001])

The plasma torch is divided into two main pieces, a positive portion and a negative portion. The body insulator, labeled part I, insulates the two sides from each other. With the exception of the cathode, labeled part C, the positive portion consists of all of the parts to the left of the body insulator. The negative portion of the torch includes all of the parts to the right of the body insulator as well as the cathode. The two sections are joined by bolts, not shown, threaded into part B that are surrounded with insulating jackets to isolate the two halves.

A cylinder of compressed nitrogen is used as the feedstock supply, which is attached to the plasma torch using the feedstock supply tube, labeled part K. The feedstock then flows through the flow swirler, labeled part F, which produces the angular momentum that is used to spin the arc around the electrodes. The arc is struck between the negatively charged cathode, labeled part C, and the positively charged anode, labeled part A. Because of the careful alignment of the electrodes and the low pressure through the middle of the constrictor (the small opening shown on the far left of the anode), the arc travels through the constrictor and attaches on the outside of the anode.

The gap between the electrodes is adjusted using the micrometer drive, labeled part D. The arc length is the distance through the constrictor plus the electrode gap. The length of the arc determines the voltage necessary to strike the arc, while the current

20

determines the diameter of the arc. The electrode gap was adjusted by first moving the cathode until it was in contact with the anode. The cathode was then moved away from the anode until an ohmmeter showed a break in contact. The cathode was then moved back a further 0.1778 mm (0.007 in). This electrode gap was determined by Gallimore to give the best performance of the torch with a nitrogen feedstock.

The materials used for a plasma torch are very important. The electrode material must be able to strike an arc easily and withstand the high temperatures of the arc. In this torch, thoriated tungsten was used for the cathode, part C. The thorium improves the ability of the electrode to strike an arc, while the tungsten is a tough, high-temperature material. The anode, part A, was made of copper. Copper was chosen because it is both a good electrical and thermal conductor, and it is not eroded quickly when nitrogen is used as a feedstock. The torch body, part B; micrometer bracket, part E; and micrometer drive, part D, were made from stainless steel to withstand the heat from the arc. The body insulator, part I; flow swirler support rod, part G; and bolt insulators were made from PEEK, a high temperature plastic with good insulating properties. The flow-swirler, part F, was made from boron-nitride, a machinable ceramic. Boron-nitride could withstand the higher temperatures experienced near the electrodes better than PEEK, which was used farther away from the electrodes.

The power supply system for the plasma torch is shown in Figure 3-3. Three constant-current arc-welding power supplies connected in series supply power to the torch. A burst of high-frequency voltage is needed to start the arc. Once the arc is started, the voltage from the arc-welding power supplies is sufficient to keep the arc established. In practice, only a 0.25 second burst of the lowest-intensity high-frequency voltage is needed to start the arc.
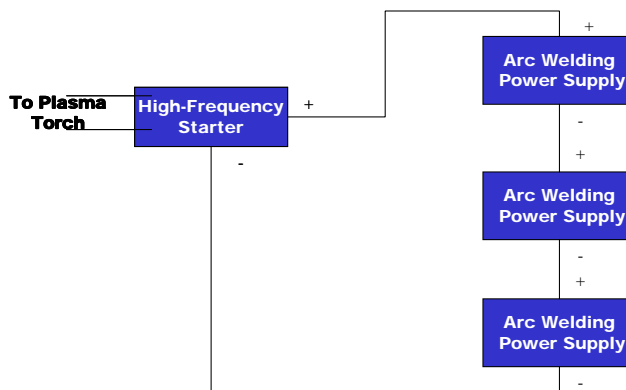
Figure 3-3: Schematic of Plasma Torch Power System

Each of the arc welding power supplies used provides an open circuit voltage of 67 V. The entire power supply system, therefore, provides a total open circuit voltage of 201 V. Once the arc was started, the current provided by the power supply system was in the range of 30 to 40 A. The power supplies would then regulate the voltage to maintain a constant current. Typically, the voltages were around 40 to 50 V during the operation of the torch.

The computer used to control the wind tunnel was also used to control the power supply system. Both the arc-welders and high-frequency starter have remote switches to turn them on and off. These switches are controlled by digital relays that are controlled by the wind tunnel control computer. The welders are turned on at the beginning of the wind tunnel run, but will not usually produce an arc until the high-frequency voltage is applied. The high-frequency starter is operated by turning on the digital relay controlling the remote switch of the high-frequency starter for 0.25 second.

3.1.3 Flow System

All gases needed for the setup were provided by compressed storage cylinders that were regulated to the desired pressure. Nitrogen was used as the torch feedstock gas as well as for purge of the fuel system. Ethylene was used as the fuel to the strut. A schematic of the flow system is shown in Figure 3-4. Manual valves were used to turn the flow from each of the cylinders on and off. The fuel and nitrogen purge were

connected to a three-way valve. The three-way valve allowed nitrogen to flow through the system, except when the fuel was turned on by the three-way valve. The three-way valve used compressed air to switch between the ethylene and nitrogen. The compressed air valve could then be turned off to purge the system with nitrogen. This method of controlling the fuel flow allowed manual shutoff of the fuel at any time during a wind tunnel run.
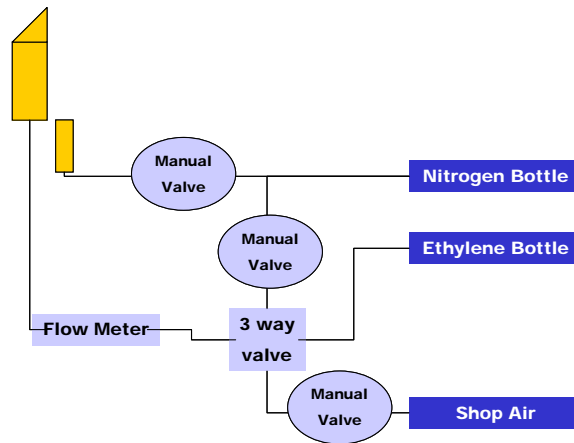
Figure 3-4: Schematic of the flow control system

3.1.4 Supersonic Wind Tunnel

All tests were performed in the Virginia Tech supersonic wind tunnel facility, shown in Figure 3-5. The test section of this facility has a 230 mm (9 in) square cross-section by 300mm (12in) long. Various nozzles can be used to achieve different Mach numbers in the test section. For all tests in this study the Mach number of the flow was 2.4. The wind tunnel is unheated so the static temperature of the flow is near 150 K, with a total temperature of 300 K. The total pressure of the flow was 344 kPa (3.4 atm) for all tests.

Figure 3-5: Picture of Virginia Tech Supersonic Wind Tunnel

The wind tunnel is a blow-down facility, which operates by pumping a number of holding tanks to a high pressure and then releasing that air through the tunnel. The tunnel flow control system consists of two valves. The first valve is a butterfly valve that simply opens or closes. The second valve is a hydraulically controlled valve that regulates the total pressure of the settling chamber. Typical runs of the wind tunnel are 14 to 20 seconds long.

A picture of the wind tunnel test section with the strut and plasma torch installed as used in the current study is shown in Figure 3-6. The plasma torch is mounted in the floor of the wind tunnel just behind the strut in the picture shown. To achieve different positions of the strut relative to the plasma torch, the strut could be mounted in different positions on the wind tunnel floor plate. Two different placements of the strut were tested. The first, at a distance equal to a single strut thickness was as shown in the picture. The second was with the strut mounted 2 strut-thicknesses (13 mm) upstream of the plasma torch. The traverse probe was located 12 strut- thicknesses (76 mm) downstream of the plasma torch for all tests.

24
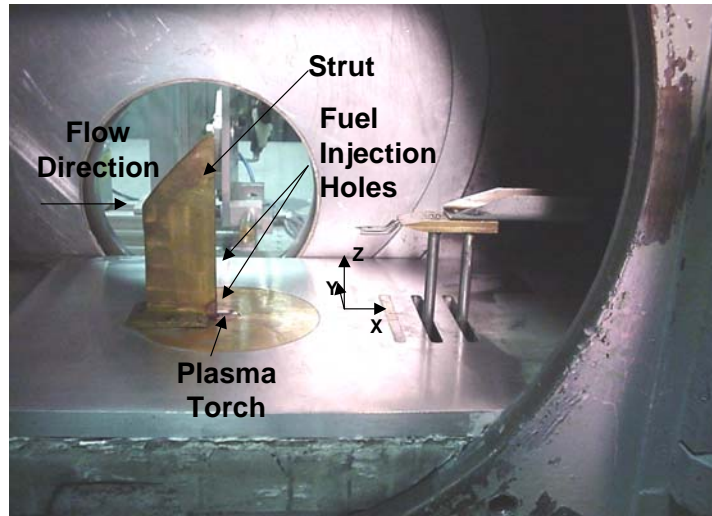
Figure 3-6: Photograph of wind tunnel setup

3.2 Measurement Systems

Several measurement systems were used to gather information during a run. The measurement systems that provided data on the flow are shown in Figure 3-7. All of the measurements were taken using two personal computers equipped with data acquisition systems. A discussion of the uncertainty of the measurement systems is included in Appendix B. In the following, the first of three sections will discuss the systems operated by the wind tunnel control computer. The next section discusses the spectrometer and its control system. The final section discusses the video and photography system used in testing.
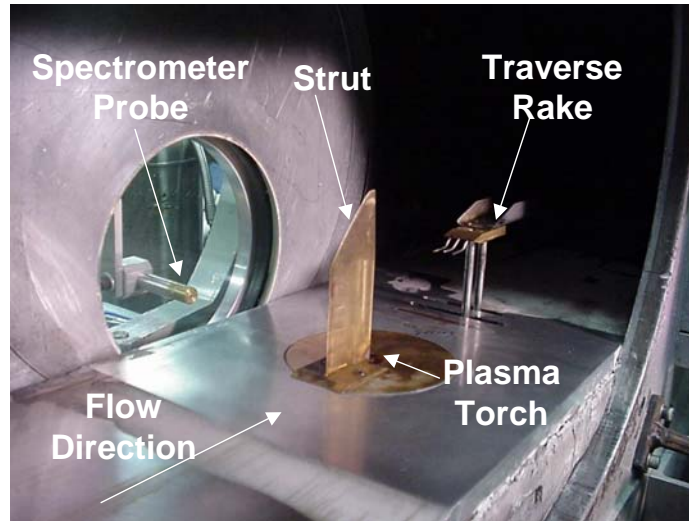
Figure 3-7: Location of measurement systems in wind tunnel test section

3.2.1 Wind Tunnel Control and Measurement System

All measurements, except for the spectrometer were taken using the wind tunnel control computer. The main component of the data acquisition system was a multiplexer board that would allow the 8-channel data acquisition system in the wind tunnel computer to accept 32 channels of data. The multiplexer board also had an onboard cold junction compensator for thermocouple inputs. The wind tunnel control and data acquisition programs were done in LabView. A block diagram of the entire measurement system is shown in Figure 3-8.
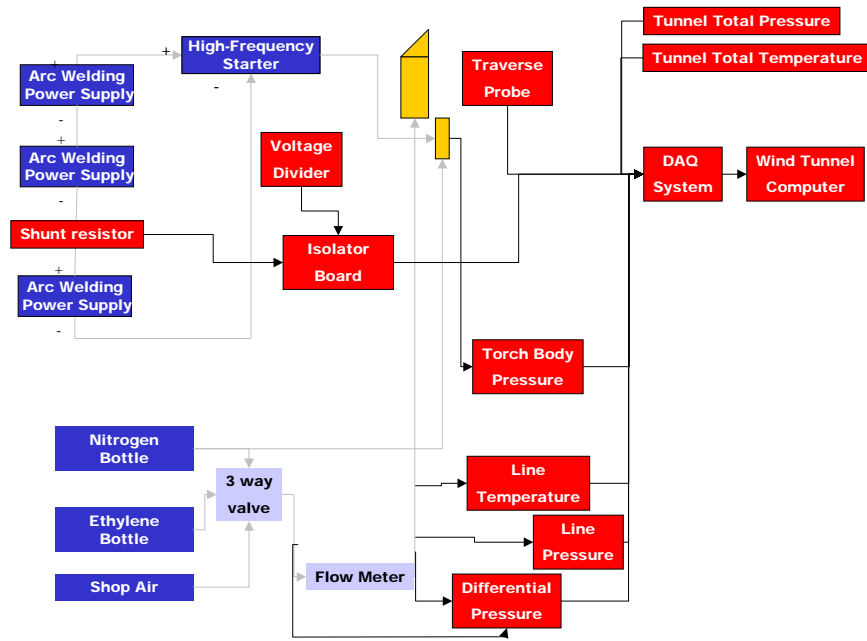
Figure 3-8: Block Diagram of the measurement systems used

In order to determine the power to the plasma torch, both the voltage and current to the plasma torch must be measured. The voltage supplied to the plasma torch is measured at the high-frequency starter by using a 100 to 1 voltage divider circuit that is connected to the wind tunnel data acquisition system. Before going to the wind tunnel computer data acquisition system, the voltage signal is run through an isolator to prevent high levels of potentially damaging electrical noise caused by the high-frequency starter from reaching the data acquisition system. The current is measured by using a shunt resistor in one of the cables connecting the arc-welders. This shunt resistor has a known voltage drop of 1mV per amp of current through the resistor. This voltage also runs through an isolator before going to the tunnel data acquisition system.

The pressure of the feedstock supplied to the torch was measured with a pressure tap in the body of the torch. The torch feedstock pressure is important because it determines the mass flow rate of feedstock through the choked nozzle of the torch. Also, the pressure affects the characteristics of the arc in the torch.

The flow rate of fuel was measured using an orifice-type flow meter. In order to calculate the mass flow rate the fuel line pressure, the pressure drop across the orifice and

27

temperature of the fuel must be measured. The properties of the fuel, based on the values measured at the flow meter, can then be calculated using curve fit data.

A stepper motor traverse system was used to sample data within the flow. For all of the testing done in this study the traverse rakes were located 12 strut thicknesses (75 mm) downstream. Two different traverse rakes were used to sample the flow in this study.

The first rake had three total temperature probes, and is shown in Figure 3-9 (a). This allowed a survey of the total temperature in a downstream plane to be done quickly. The probe design is shown in Figure 3-9 (b). A thermocouple is routed through the probe to the tip, which is open to the flow. Four holes are drilled around the circumference of the probe. The main goal of the thermocouple probe design was to maximize the recovery factor of the probe. The recovery factor of this probe has been measured to be 0.98[Jacobsen, 2001].

(a)   (b)
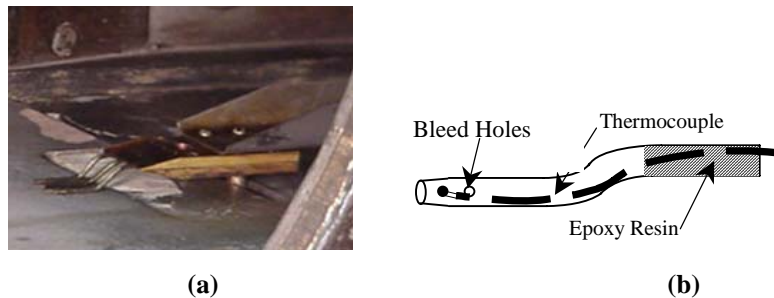
Figure 3-9: Schematic (a) and picture (b) of total temperature probe

Because the total temperature probe was able to measure the total temperature at three different locations at the same time, a fairly fine grid of measurements could be taken. The plane of measurement can be seen in Figure 3-10. The forty measurements of the total temperature were recorded at each of thirty stations. The traverse reached a height of 9.8 strut widths. The probe would then be moved 0.25 strut thicknesses in the spanwise direction for the next run. In all, five good tunnel runs were necessary to assemble a set of data.

28
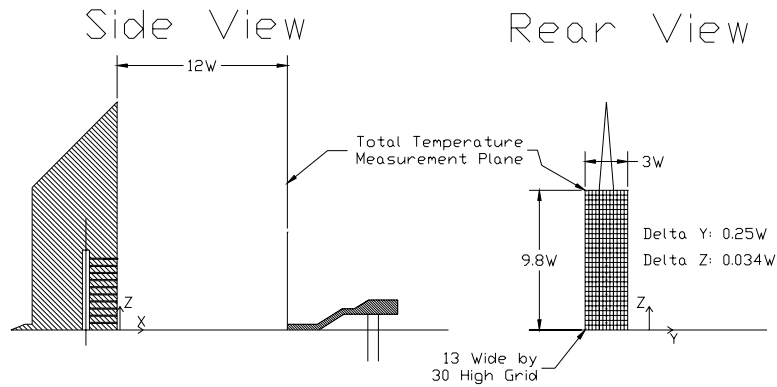
Figure 3-10: Schematic of Total Temperature Measurement Plane

The second traverse rake had three probes, a total pressure probe, a total temperature probe and a cone-static probe. These three measurements allowed the Mach number, density, and enthalpy of the flow to be calculated. Details of the data reduction are given in Appendix B. A picture of this rake is shown in Figure 3-11. The cone-static probe had a ten degree half-angle, with four ports arranged around the circumference of the probe. The total pressure probe had an interior diameter of 1.04 mm. The total temperature probe was identical those in the total temperature rake described above.
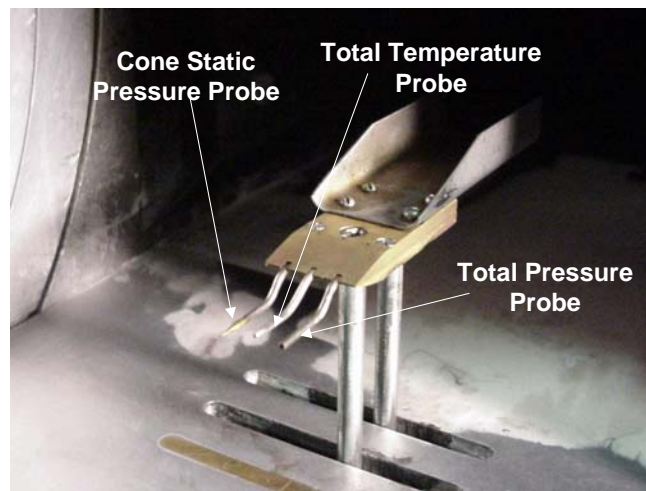
Figure 3-11: Photograph of triple probe rake

Because the triple-probe rake had three different probes, the rake had to be moved in such a way as to get all three measurements at the same location. Therefore, a coarser grid was used in the spanwise direction for these tests. This grid is shown in Figure 3-12.

29

Triple probe rake measurements were taken up to 7.7 strut widths high, with one-half strut width between spanwise measurement locations.
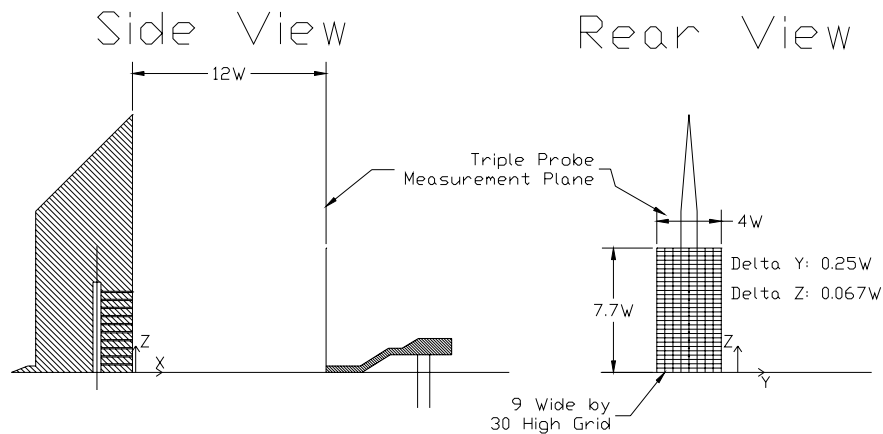
Figure 3-12: Triple probe rake measurement plane

3.2.2 Spectrometer Measurement and Control System

Spectroscopic measurements of the tests were taken using a three-channel Ocean Optics S2000 spectrometer. Three channels allowed measurement to be taken between 196nm to 730 nm, while maintaining good spectral resolution by allowing one spectrometer to take data over a third of the total wavelength range. Photons entered the measurement system through a scope that was connected to a fiber optic cable. This single fiber optic cable was then split with a trifurcated splitter into three fiber optic cables. These three cables then went to separate channels of the spectrometer. Unfortunately, one of these three cables was broken coming out of the trifurcated splitter. Therefore, only the two spectrometers at the lower end of the wavelength spectrum were used for the reported measurements.

The spectrometer scope was attached to two precision positioning stages to allow the spectrometer to be positioned in two dimensions. These stages were mounted to an optical table. The positioning stages with the spectrometer attached are shown in Figure 3-13. In the original series of tests, the placement of the wind tunnel window prevented the spectrometer from being able to view areas very far downstream. To help alleviate this problem the spectrometer was positioned at a ten-degree angle to the wind tunnel.

This ten-degree angle allowed the spectrometer to view areas farther downstream without distorting the measurement path appreciably. In later tests, when the triple probe rake was used, the strut and plasma torch were moved forward in the test section, eliminating this problem.
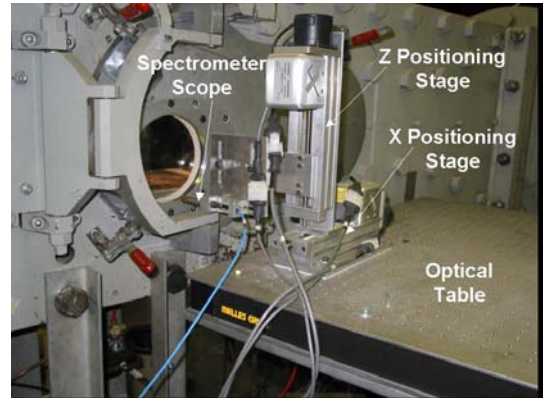
Figure 3-13: Spectrometer Scope and Positioning System

For a typical wind tunnel run, the spectrometer would be set to average two measurements with 100 ms integration time at each measurement location. During the run, the spectrometer would index in the vertical direction, taking measurements at 8 locations. The spectrometer would then be indexed in the streamwise direction between runs. In the first series of tests, the distance between vertical stations was 5mm and the distance between horizontal stations was 6.25 mm. During the second set of tests the spectrometer was indexed 2mm in the vertical direction, and 2mm in the streamwise direction between runs. These two measurement planes are shown in Figure 3-14.

First Set of Tests   Second Set of Tests
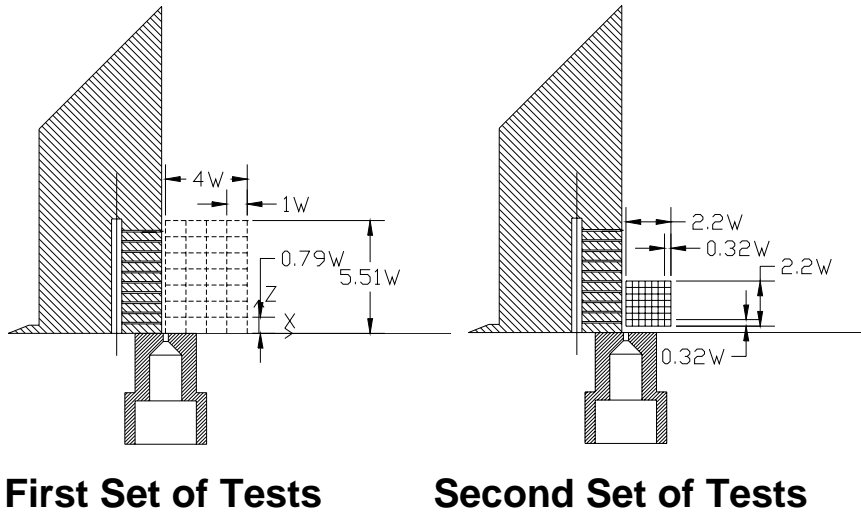
Figure 3-14: Spectrometer measurement planes for both series of tests

3.2.3 Filtered Photography and Video

All wind tunnel runs were video taped. The video could then be used to diagnose problems. Also, still pictures could be captured through a video capture card on a computer. A 35mm camera was used to take photographs of the wind tunnel runs. Photographs could be taken either with or without lens filters. The lens filters used eliminated all but a small range of wavelengths of light. The bands of wavelengths that were passed through the filter were chosen to correspond with the emissions from species participating in the combustion process.   The filters used are listed in Table 3-1 with the center wavelength, the range of wavelengths that were transmitted, and a typical shutter speed. The shutter speed and aperture setting of the camera were adjusted to expose the film enough to get a clear picture.   Typically during a run, three pictures would be taken with the aperture completely open and at different shutter speeds.

32

Table 3-1: Spectral Filter Specifications

Filter Type	Manufacturer	Center Wavelength	Transmission Range	Transmission Efficiency	Shutter Speed
OH	Ealing-Electro Optics	310.0 nm	10.0 nm	Not Provided	1/4
H	Ealing-Electro Optics	656.7 nm	11.1 nm	54%	1/500
C_2	Ealing-Electro Optics	515.1 nm	8.8 nm	52%	1/500
CH	Ealing-Electro Optics	431.4 nm	8.1 nm	46%	1/250

3.3 Test Procedures

This section discusses the testing done and the procedures followed during those tests. The first section discusses the test matrix. The second section describes a typical test run and the criteria for a good run.

3.3.1 Test Matrix

All testing was done in an unheated Mach 2.4 flow with a freestream total pressure of 345 kPa (3.4 atm). Three different configurations of the strut and plasma torch were tested. The first two setups had the plasma torch placed just downstream of the torch. The first configuration, referred to as Configuration A, had all of the fuel injection holes the same diameter of 0.508mm. The second configuration, Configuration B, had the bottom four holes drilled out to a diameter of 0.711mm. The third configuration, Configuration C, used the same strut design as Configuration B, but the strut was moved upstream of the plasma torch two strut-thicknesses (12.7mm).

Besides the configuration of the setup, fuel flow and the plasma torch power were varied. The power of the torch was varied from 1500W to 2500W. The mass flow rate

of fuel injected through the strut was varied from 0 g/s to 2.23 g/s. The entire test matrix is given in Table 3-2.

Table 3-2: Test Matrix

Total Temperature Rake Tests

Configuration	Power	Mass Flow Rates of Fuel
A	1500	0g/s, 0.68g/s, 1.28g/s, 1.67g/s, 2.17g/s
B	1500	0g/s, 0.651g/s, 1.68g/s, 2.23g/s
B	2000	0g/s, 0.651g/s, 1.68g/s, 2.23g/s
B	2500	2.23g/s
C	1500	0g/s, 0.54g/s, 1.64g/s, 2.20g/s

Triple Probe Rake Tests

Configuration	Power	Mass Flow Rates of Fuel
B	1500	0g/s, 2.23g/s
B	2000	0g/s, 2.23g/s
B	0	0g/s

Initially, a total temperature survey was done with Configuration A to evaluate how well the setup worked. Configuration B was designed to improve the results from the testing of Configuration A. Configuration C was an attempt to see how the placement of the strut with respect to the plasma torch affected the results. Configuration B was determined to be the best configuration, so it was investigated more fully with the triple probe rake over a limited range of powers and fuel flow rates.

3.3.2 Typical Test Procedure

This section explains the usual procedure and order of operation during a typical wind tunnel run. First, the nitrogen used as a feedstock and fuel purge was turned on. The video camera was started to record the entire run. The wind tunnel was then started. After the tunnel had run for one second, the plasma torch was started. As soon as the plasma torch started, the fuel was turned on. The system was then allowed to stabilize for one second. The aerothermodynamic sampling traverse was started at the same time as the spectrometer. Also, any pictures that needed to be made were taken while the other measurements were being made. Once both the tunnel traverse and the spectrometer had

finished making measurements, the plasma torch was turned off. The fuel was turned off after the plasma torch went out. The tunnel then ran for an additional one to two seconds and was shut off.

A tunnel run was considered satisfactory if it met three criteria. First, the freestream tunnel pressure had to be within ± 10% of the desired level throughout the test. Second, the torch power had to be within ± 5% of the nominal level. The power tended to drift over time due to the wearing of the plasma torch electrodes. Third, the fuel mass flow rate had to be within ± 5%. The fuel mass flow rate tended to be very stable and needed little adjustment.

Chapter 4: Aerothermodynamic Sampling Results

This chapter presents the results from the two traverse rakes discussed in Chapter 3. The first rake used was the total temperature rake. Contour plots and vertical profiles of total temperature ratios are discussed in Section 4.1. Next, the results from the pressure rake are discussed in Section 4.2. The use of the pressure rake allowed a more detailed study of the flow. This increased detail permitted the important properties of the flow to be calculated, and these results are presented in that section.

4.1 Total Temperature Sampling

Total temperature data was taken as described in Chapter 3. As previously discussed, the three-probe total temperature rake allowed the total temperature downstream of the strut to be surveyed with fewer wind tunnel runs. Early tests were done with Configuration A, which had all fuel injection holes the same size. These early tests showed the area of maximum temperature away from the plasma torch and the bottom of the strut. Therefore, the diameter of the bottom fuel injection holes was increased to increase the amount of fuel flow near the bottom of the strut to make Configuration B. After testing Configuration B, the strut was moved upstream two strut thicknesses, to Configuration C, to evaluate how the placement of the plasma torch relative to the strut affected the performance of the system.

All three configurations were tested with different flow rates of fuel. Configuration B was tested with different input powers to the plasma torch. The results will be presented first in a qualitative sense in contour plots. The results will then presented in a more quantitative sense in plots which are along the line of maximum temperature.

4.1.1 Total Temperature Contour Plots

Total temperature ratio contour plots, which are the total temperature measured at the probe divided by the free stream total temperature, are presented in this section for all of the configurations tested. Because the freestream total temperature of the supersonic wind tunnel would change both during a run and as the weather changed during testing, the total temperature ratio was used to evaluate the tests. The data acquisition system took 30 measurements at each Z position. The probe total temperature was calculated from the average of the last five data points to allow the probe time to respond to temperature changes. The averaged total temperature at the probe was then divided by the average of the freestream total temperature measured at the same time.

The results for the tests of Configuration A with various mass flow rates of fuel and a plasma torch power of 1500W are shown in Figure 4-1. The plasma torch alone produces little heating of the flow. As the amount of fuel injected is increased, the temperature rise is increased significantly. At the maximum flow rate of 2.17 g/s of fuel, there is a 10% increase in temperature over that of the freestream. An increase in the total temperature with an increase in the mass flow rate of the fuel is an important result, because it shows that more heat release is occurring when more fuel is present. This result means that the plasma torch is causing some exothermic reaction with the fuel.
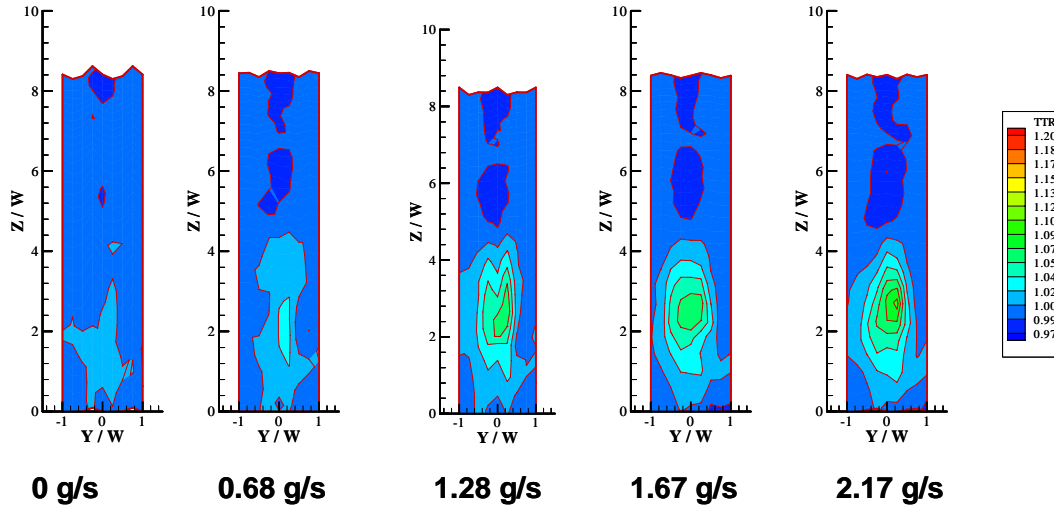
Figure 4-1: Contour plots of total temperature ratio for Configuration A with P = 1500 W and varying fuel flow rates

Additionally, all of the plots above show the area of fuel-produced temperature rise well above the level of the tunnel floor and the exit of the plasma torch. Comparing the plasma-torch-only case to the other cases, it can be seen that the energy from the plasma torch remains fairly close to the floor of the wind tunnel. Therefore, the area of temperature rise moving above the floor of the wind tunnel when fuel is present must result from the delivery of the fuel. Two possible causes for the temperature rise occurring at increased levels from the wind tunnel floor are (1) that more fuel is being delivered to the higher fuel injection holes or (2) that the plasma torch is blocking the fuel flow from the bottom holes. With the simple injection scheme used in the strut, there could be a significant difference in the amount of fuel being delivered from each of the holes. Therefore, the fuel delivery was varied to produce Configuration B, as will be discussed below. The second possibility is that the flow from the plasma torch could be blocking the flow from the bottom fuel injectors. This blockage would cause more fuel to flow from the top fuel injectors and could cause the results seen.

Even though the temperature rise starts well above the floor, the area of temperature rise does not extend to the top fuel injection hole. The highest fuel injection hole is 5.4 strut widths from the floor of the tunnel, while the temperature rise is only seen to about 4.5 strut widths above the floor. The temperature rise may not be extending

38

to the top fuel injection hole because the fuel from the lower fuel injection holes shields the plasma from the fuel from the highest injection holes. These results show that the fuel delivery scheme could have a large impact on the interaction of the fuel with the plasma.

In all cases the area of temperature rise is slightly off the centerline of the strut. This shift could be due to a number of factors. The strut could be slightly asymmetrical or installed at a slight angle of attack to the flow, causing the wake behind the strut to be off center. Another possible cause of the heat release being off center is that the fuel injection holes could have been drilled at slight angle to the back of the strut, causing the fuel to be sprayed off center. A final possibility could be that the fuel injector plasma torch interaction causes the area of temperature rise to shift off center.

After the preliminary testing of Configuration A, the bottom four fuel injection holes were enlarged by 40% to 0.711mm to make Configuration B. This change was made to see how changing the pattern of the fuel delivery would affect the amount and location of the temperature rise. The larger holes should increase the amount of fuel near the wind tunnel floor, while decreasing the velocity of the fuel jets. Decreasing the velocity of the fuel should help the plasma to penetrate through the fuel from the lower injectors.

The first results for Configuration B are all with the plasma torch off, and they are shown in Figure 4-2. The first plot is for the strut with no injection through the strut or the plasma torch. The second has a nitrogen purge through the fuel injector holes. These plots give a baseline against which to compare the later plots. From these plots, the wake of the strut is noticeable because of a drop in total temperature caused by the vorticity in the wake. The same effect was seen in the aeroramp work as discussed by Jacobsen [2001].   The wake is more pronounced when the purge is injected from the strut. This larger temperature drop could be caused by an increase in the effect of the wake downstream caused by the injection, or because the purge was colder than the rest of the flow. From these plots, both the wake of the strut and the injection of the purge from the strut appear to be on the centerline of the strut. This result indicates that the temperature rise occurring off the centerline as seen in Configuration A and later with this configuration was due to an interaction of the plasma torch and the fuel injection.

Strut Only   Strut and Purge
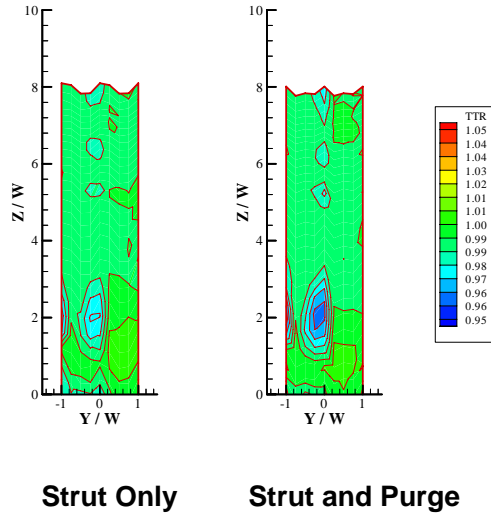
Figure 4-2: Contour plots of total temperature ratio for Configuration B without the plasma torch

Shown in Figure 4-3 are the plots for Configuration B with 1500 W plasma torch power and varying mass flow rates of fuel. Again, both the area of temperature rise and the maximum total temperature ratio increased with an increase in the mass flow rate of fuel. The area of temperature rise does not appear to move any closer to the location of the top fuel injector than it did for Configuration A. The magnitude of temperature rise for Configuration B is higher and appears to be more concentrated than it was for Configuration A. One reason for this could be that the larger holes in the bottom of the strut deliver more fuel to an area where it can interact with the plasma, and the effects of the plasma cannot reach the location of the highest fuel injector.
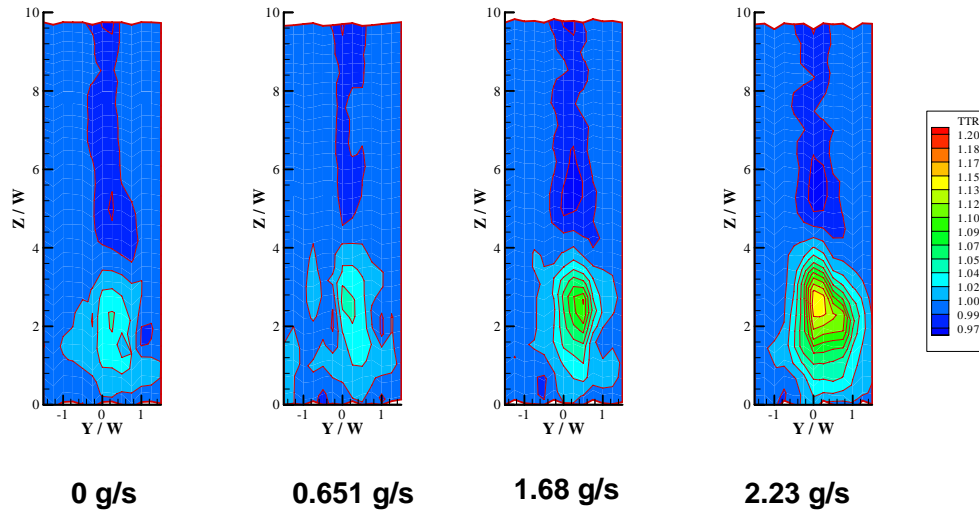
Figure 4-3: Total temperature ratio contour plots for Configuration B with P = 1500 W and varying fuel flow rates

Figure 4-4 shows the temperature plots for Configuration B with 2000 W power to the plasma torch and varying mass flow rates. Again, trends similar to the 1500 W cases are seen as the mass flow rate is increased. The total temperature ratio does increase for the 2000 W case over what was seen for the 1500 W case. However with just these results, it is difficult to say if the temperature rise seen is due only to the additional power to the plasma torch heating the flow, or if it is due to a more intense reaction of the fuel with the plasma.

41

0 g/s   0.651 g/s   1.68 g/s   2.23 g/s
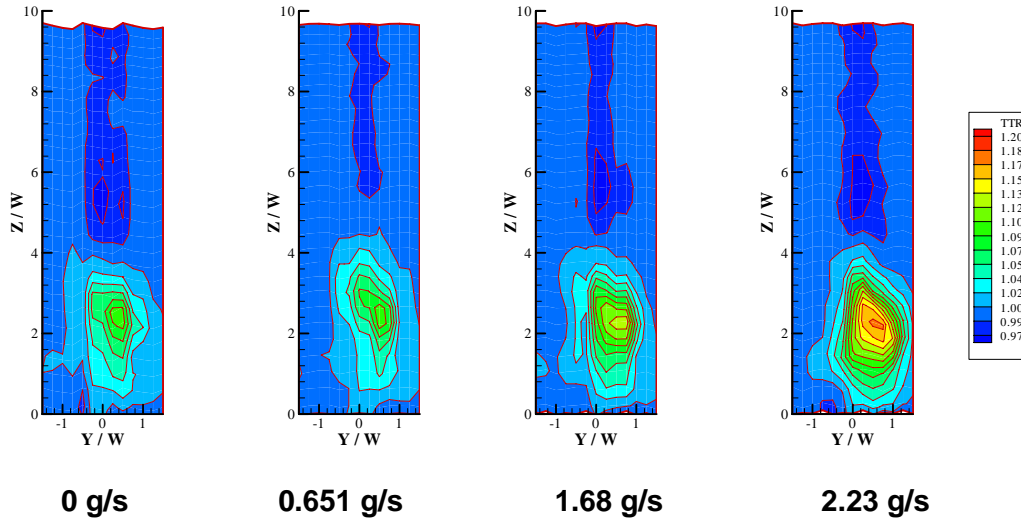
Figure 4-4: Total temperature ratio contour plots for Configuration B with P = 2000 W and varying fuel flow rates

Contour plots comparing Configuration A and B at the same mass flow rates are shown in Figure 4-5. The first noticeable difference between the plots is the width of the measurement areas on the x-axis. A smaller measurement plane was used for Configuration A in order to allow fewer wind tunnel runs. The second difference seen is that the area of temperature rise moved closer to the wind tunnel floor when the diameter of the bottom holes was increased. However, the area of reaction is still well above the floor. This result indicates that the flow from the plasma torch is blocking the fuel flow from the bottom fuel injectors. The change to Configuration B not only caused an increase in the area of temperature rise, but also increased the maximum temperature seen. This increase in temperature is most likely caused by having more fuel in the area where the fuel and plasma torch interact. Fuel injected from the top fuel injectors continues to show no reaction with the plasma. The fuel from the top injectors likely does not react with the plasma, because the fuel from the lower fuel injectors shields the plasma from the fuel from the higher injectors.
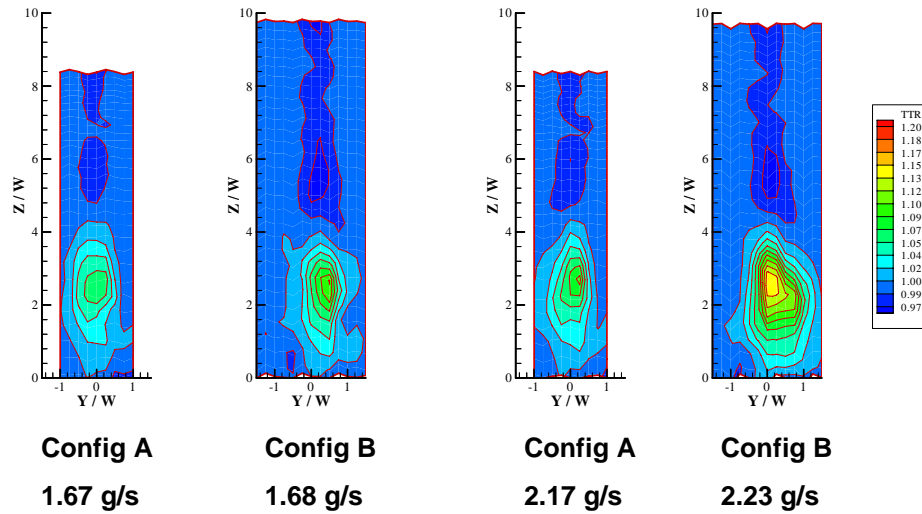
Figure 4-5: Configuration A compared to Configuration B with P = 1500 W similar fuel flow rates

Figure 4-6 shows the contour plots for Configuration B with different power levels and the same mass flow rate. The scale for the contour legend is different from the earlier plots because of the larger temperature rise caused by the 2500 W torch power. As the power is increased, both the maximum temperature rise and areas of temperature rise increase. However, as noted above, it is difficult to say with just these results whether the increase in temperature rise is due to an increase of the reaction of the plasma with the fuel or if it is purely due to the increased energy from the plasma torch heating the flow. The spectrometer results presented in the next chapter will provide insight on this question.

1500 W **2000 W** **2500 W**
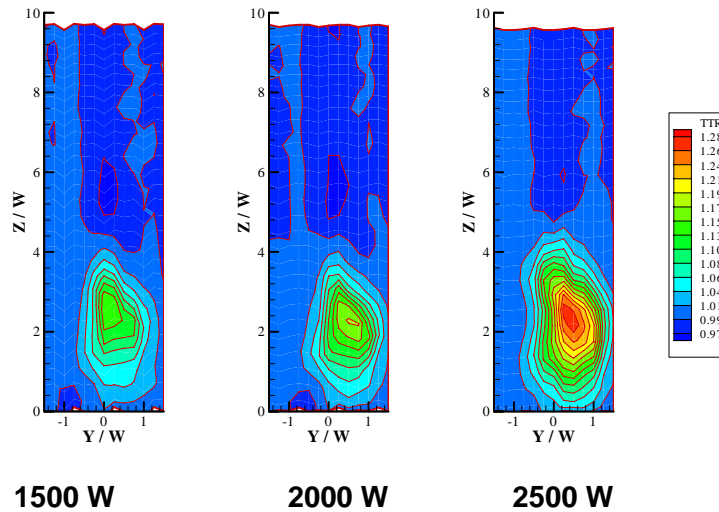
Figure 4-6: Total Temperature ratio contour plots for Configuration B with a fuel flow rate of 2.23 g/s and varying powers

Configuration C had the same fuel injection hole pattern as Configuration B, but the strut was moved upstream of the plasma torch two strut-thicknesses. This configuration allowed the placement of the strut-flameholder relative to the plasma torch to be studied. Figure 4-7 shows Configuration C with the plasma torch off and various test conditions. The strut-only case shows the lower temperature in the wake as seen earlier. The wake is centered on the origin with the exception of an area near Z/W equal to 2. This area is most likely caused by an imperfection in the wedge. The addition of the purge gas increases this disturbance. The addition of the feedstock flow creates a disturbance on the other side of the figure. This shows that there is an interaction between the fuel injection and the injection from the plasma torch.
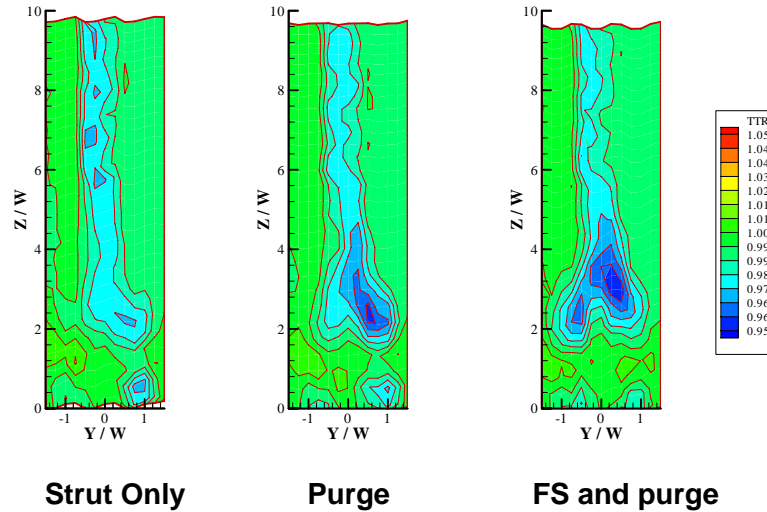
Figure 4-7: Total temperature ratio contour plots for Configuration C with no power to the plasma torch

The temperature contours with fuel injection and 1500 W plasma torch power are shown in Figure 4-8. The color scale of the contours has been adjusted from that of Configuration B to better show the differences in temperature rise seen. Configuration C has a much lower temperature rise than Configurations A or B. This difference is attributed to two main factors. The first cause is that the fuel starts to mix with the air and less is concentrated near the plasma torch. The second cause is that the strut is no longer serving as the flameholder. The strut injects the fuel out away from the floor of the wind tunnel into the flow, but the plasma torch is no longer located in the wake region of the strut. Therefore, the plasma torch is serving as the flameholder, and it is not as effective of a flameholder as the strut. However, moving the strut upstream appears to improve the penetration of the plasma into the flow. This result will be discussed more in the next section.
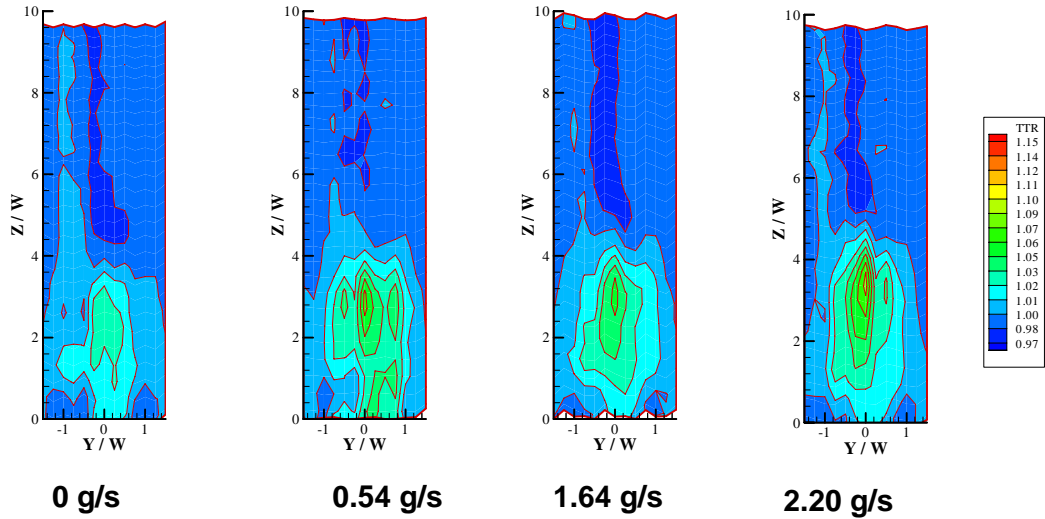
Figure 4-8: Total temperature ratio contours Configuration C with P = 1500 W and varying fuel flow rates

Another noticeable difference between the results for Configurations A and B and those for Configuration C is that the temperature rise is located at the centerline of the strut. This result is logical because the plasma torch is near the center of the strut. Therefore, only the fuel injected near the centerline of the strut was ignited. The reaction of only part of the fuel is another possible reason that the overall temperature rise is not as great for Configuration C as for the other configurations.

4.1.2 Total Temperature Profiles

In this section total temperature profiles, with some additional plots to summarize the results discussed in this section and the previous section are shown and discussed. These plots serve to give a more quantitative measure of the differences seen in the contour plots discussed above. The majority of the plots are centered along a line at Y/W equal to 0.25. This location is a good location for comparing Configurations A and B, because the temperature rise occurred off the centerline. Configuration C had most of the temperature rise on the centerline, but some of the plots will be shown on the 0.25 Y/W line.

Figure 4-9 shows the total temperature ratio profiles for Configuration A at 1500 W and various mass flow rates of fuel. As the fuel flow rate increases, the maximum temperature increases, except for the 1.67 g/s case, which is slightly lower than the 1.28 g/s case. However, looking back at the contour plots shown in Figure 4-1 the area of temperature rise is larger for the 1.67 g/s case. Therefore, the fuel must be spreading better at this mass flow rate than for the lower mass flow rates. The lower velocities of the fuel due to the larger fuel injection holes cause this increase in the spreading of the fuel. The maximum temperature rise occurs at the same Z/W location for the all of the mass flow rates that show a pronounced peak. The area of temperature rise spreads downward toward the wind tunnel floor, only very little as the mass flow rate of fuel is increased. This result indicates that more of the fuel must come through a few of the holes as the mass flow rate of fuel increases, instead of the flow rate increasing through all of the holes. This difference between the holes could be caused by the plasma torch's interference effect previously discussed.
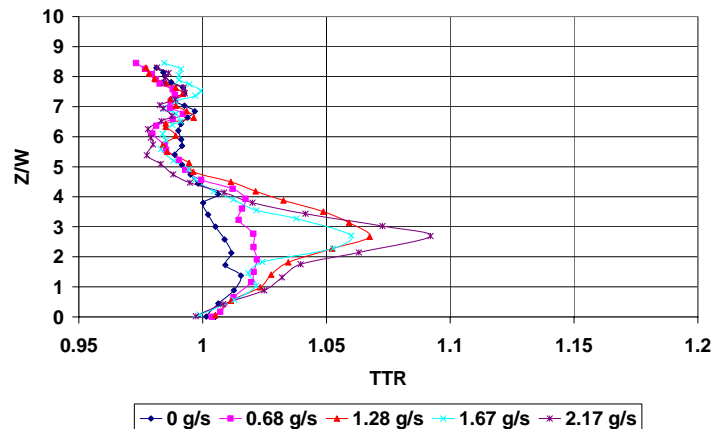
Figure 4-9: Total temperature ratio profiles for Configuration A with P = 1500 W at Y/W = 0.25 and varying fuel flow rates

The total temperature ratio profiles for Configuration B are shown in Figure 4-10. Comparing the results from Configuration B to those from Configuration A, Configuration B increased the total temperature of the freestream air 5% more than Configuration A. Also, the area of temperature rise moves toward the wind tunnel floor as the mass flow rate of fuel is increased. Configuration B moved the area of temperature

rise closer to the floor than Configuration A. This result is consistent with the modification of the bottom fuel injection holes to provide fuel flow near the wind tunnel floor. However, the temperature rise still occurs well above the floor of the wind tunnel. Therefore, only a small portion of the fuel is reacting with the plasma. Also, the reaction is not occurring near the top fuel injectors.
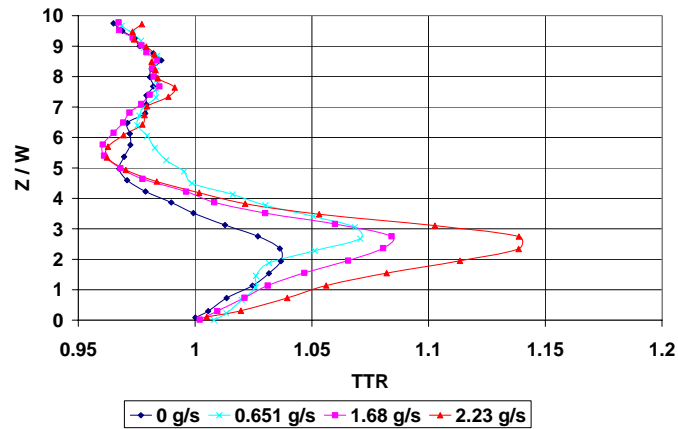
Figure 4-10: Total Temperature Ratio Profile for Configuration B with P = 1500 W at Y/W = 0.25 and varying fuel flow rates

The results for Configuration B with a power of 2000 W, shown in Figure 4-11, are similar to the 1500W results in shape, except for two differences. The first is the higher temperatures. Again, at this point, it is difficult to say what is causing the difference in temperature rise. The second difference is that the profile for the plasma torch alone shows a larger temperature rise and a fuller shape than for the lowest mass flow rate of fuel. This result could be due to the fact that the fuel is injected at a lower pressure than the purge through the injectors when no fuel is present. This lower flow through the injectors could cause the temperature rise from the plasma torch to be concentrated lower in the flow.
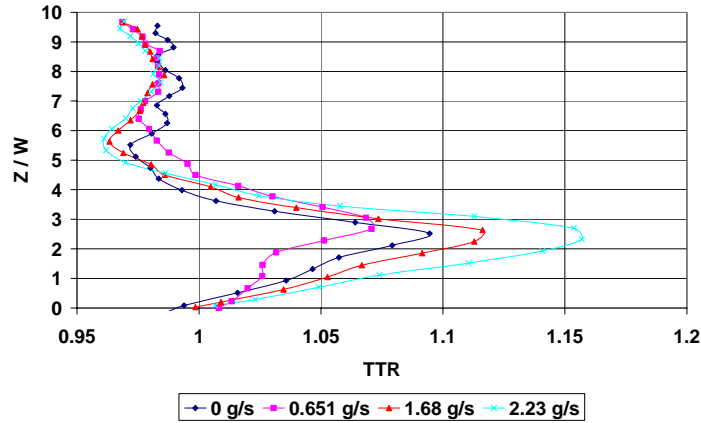
Figure 4-11: Total temperature ratio profiles for Configuration B with P = 2000 W at Y/W = 0.25 and varying fuel flow rates

The largest temperature rise for Configuration C occurred on the centerline of the strut. Therefore, the total temperature ratio profiles are presented in Figure 4-12 along the Y/W equals zero line instead of the Y/W equals 0.25 line as in the earlier cases. As was seen in the total temperature ratio contours, the total temperature rise is less for Configuration C than for Configurations A and B. However, the plasma has penetrated farther into the flow than for the other configurations. This increase in penetration height is because the flow of fuel or purge gas is causing less blockage of the plasma. However, the fuel and plasma have a smaller wake region for reaction than when the plasma torch was placed closer to the strut.
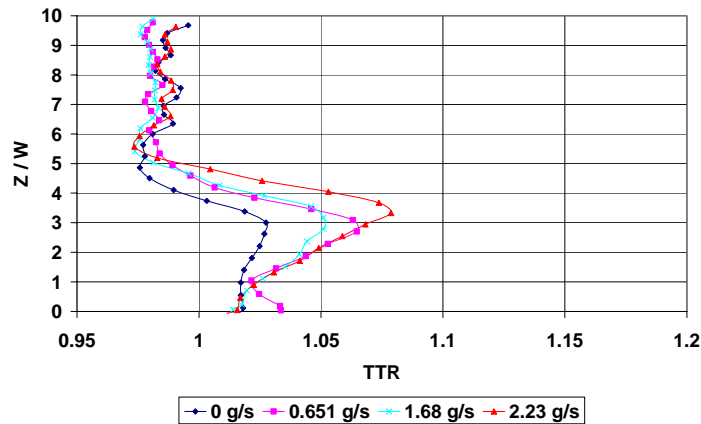
Figure 4-12: Total temperature ratio profiles for Configuration C with P = 1500 W at Y/W = 0 and varying fuel flow rates

Figure 4-13 shows the total temperature ratio profiles for the plasma torch with the nitrogen purge through the fuel injectors. All of these profiles are along the Y/W equals 0.25 line. Configuration C, which usually had a higher temperature at the strut centerline, has the highest temperature for the plasma torch alone along the Y/W equals 0.25 line. Configuration A has the lowest total temperature rise. The likely cause of this result is that there is higher velocity nitrogen injection from the bottom holes than for the other configuration. Configuration C shows a comparable temperature rise to Configuration B, but Configuration C has a fuller profile. This result is surprising because the strut is located farther away from the torch. Therefore, it seems as if the strut may reduce the performance of the plasma torch.
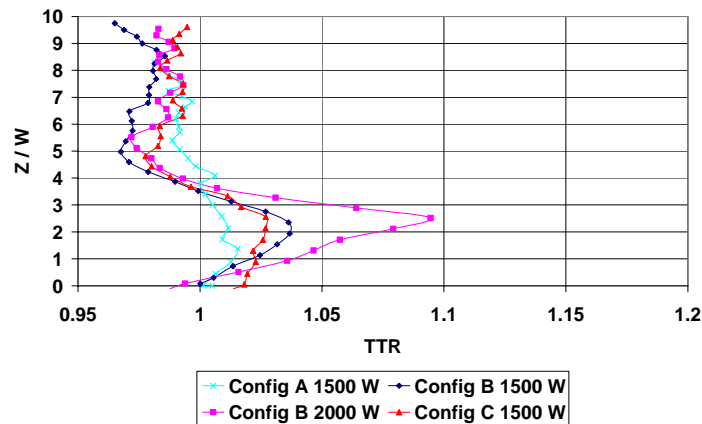
Figure 4-13: Total temperature ratio profiles for the plasma torch with varying powers and a nitrogen purge through fuel injectors at Y/W = 0.25

Figure 4-14 shows the total temperature ratio profile for a mass flow rate of fuel of 2.23 g/s of fuel and various configurations and powers. All of the profiles show a similar shape with the maximum temperature occurring at the same vertical location for all cases. Also, Configuration B has a fuller profile than Configuration A for the same power and mass flow rate of fuel. Again, there are differences between the different powers, but it is difficult to say what is causing these differences. Also, there is very little difference between the profiles for 1500 W and 2000 W. A better explanation can be made with the aid of the spectrometer results in the next chapter.
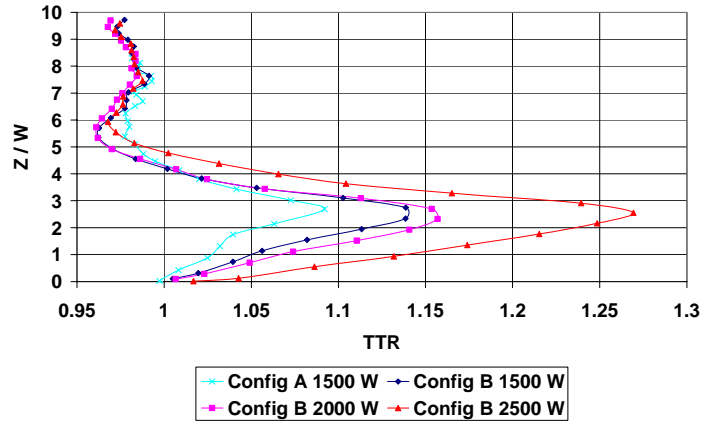
Figure 4-14: Total temperature ratio profiles for a fuel flow rate of 2.23 g/s fuel at Y/W = 0.25 and varying powers and configurations

Figure 4-15 shows a plot of the maximum total temperature ratio in each test case to summarize the results for all configurations, powers and fuel flow rates. In general, the maximum total temperature ratio increased as the mass flow rate of fuel increased. Configuration B resulted in larger temperature increases than Configuration A because more of the fuel was delivered where it could interact with the plasma. Also, increasing the power for Configuration B increased the total temperature rise. However, there is little increase in temperature rise for the 2000 W case over the 1500 W case, while there is a large difference in the temperature rise when the power is increased by the same amount from 2000 W to 2500 W. Configuration C generally performed the poorest in terms of temperature rise.

51
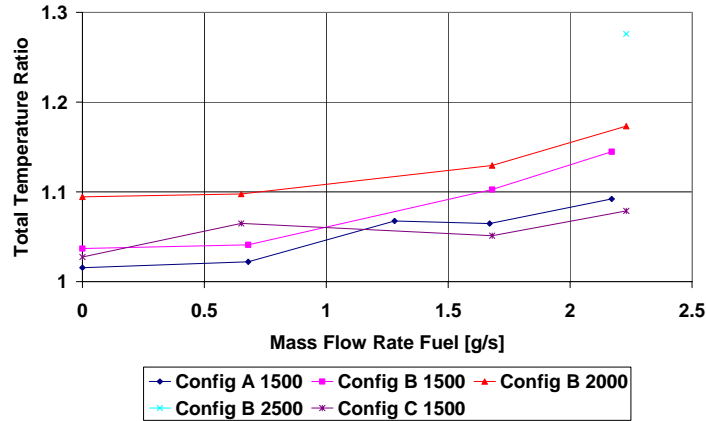
Figure 4-15: Maximum Total Temperature Ratio for all configurations, powers, and mass flow rates of fuel

An important measure of the performance of the plasma torch is how far the plasma penetrates into the flow. The penetration was quantified by the Z/W location of the maximum temperature rise. These heights are plotted in Figure 4-16. In general, the measured height of the maximum heat release increases with the mass flow rate of fuel. This effect is more related to the heat release from the fuel the heat added by the plasma jet. However, the plasma is causing the heat release to take place. The most interesting result shown in this plot is the performance of Configuration C. Even though the magnitude of the total temperature rise is fairly small, the maximum total temperature ratio occurs at a larger Z/W than for the other cases. There are two possible explanations for this result. The first explanation is that it is some sort of boundary layer effect. The boundary layer near the floor would be affected by the strut being farther upstream from the measurement location. The second possible explanation is that the fuel injection from the strut is so strong that it is bending the plasma jet in the direction of the flow. The fuel injection, then would serve to block the plasma from penetrating farther out into the flow. This may seem inconsistent with the results of the plasma torch with no fuel injection, but it must be remembered that the plasma-torch-only case still had a nitrogen purge through the fuel injectors. Another possible explanation could be that the fuel and air had longer to mix vertically and laterally with the strut farther upstream from the plasma torch
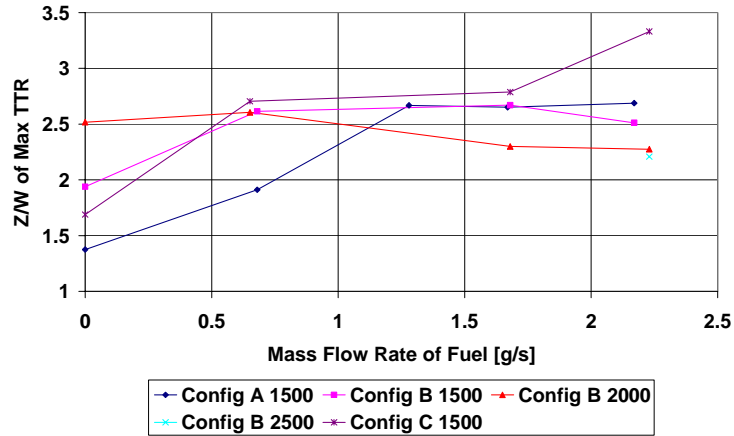
Figure 4-16: Plot of Z/W height of the maximum total temperature ratio

Because the maximum total temperature rise for Configuration C was not as large as for Configuration B, Configuration B was chosen as the configuration to be surveyed in more detail using the triple-probe rake.

4.2 Triple-Probe Rake Results

After an overall survey was done with the total temperature probe, a more detailed survey was done for a few test cases with the triple-probe traverse rake. This probe allowed all of the important properties of the flow to be calculated from the measured values of total pressure, cone static pressure, and total temperature. Four test cases were selected. The test points selected were all with Configuration B and two powers, 1500W and 2000W. Also at each power, the tests were done with the maximum flow rate of fuel and with the nitrogen purge (no fuel). Finally, as a baseline case, the fuel injection at 2.23 g/s and the feedstock supply were on, but an arc was not established in the plasma torch. This allowed the effect due to the injection of the various gases to be eliminated as a source of energy addition.

The measurements with the triple-probe rake were taken on a coarser grid than the total temperature measurements. Because each probe of the triple-probe rake had to be

located at each location where the properties of the flow were to be calculated, three runs had to be done for each measurement location in the y direction. The overall goal of this set of tests was to determine how much energy was being added to the flow by both the plasma torch and the reaction of the fuel and the plasma. These results are presented in the next two sections. The first section presents the contour plots of the measured properties of the flow. The second section describes the comparison of the measured energy release and a summation of the results.

4.2.1 Flow Property Contour Plots

Figure 4-17 shows plots of total temperature ratio measured by the triple-probe rake. The biggest difference between these results and the results for the total temperature rake measurements are the lower total temperature ratios seen in the triple-probe rake measurements. This result is discussed in more detail in the next paragraph. Another difference between the total temperature probe measurements and the triple-probe rake measurements is that the area of highest total temperature ratio for the triple-probe rake occurs along the centerline of the strut. There are no longer measurements at Y/W equal to 0.25 line that the temperature profiles discussed above were plotted on. However, the temperature rise was higher at the Y/W equal to 0.5 line for the first tests than it is for the same location with the triple probe rake tests. This result has to be a difference caused by a slight change in the experimental setup between the original set of tests and the triple-probe rake tests. Otherwise, the results appear to be similar, in that the temperature rise increases with both increased power and mass flow rate of fuel.
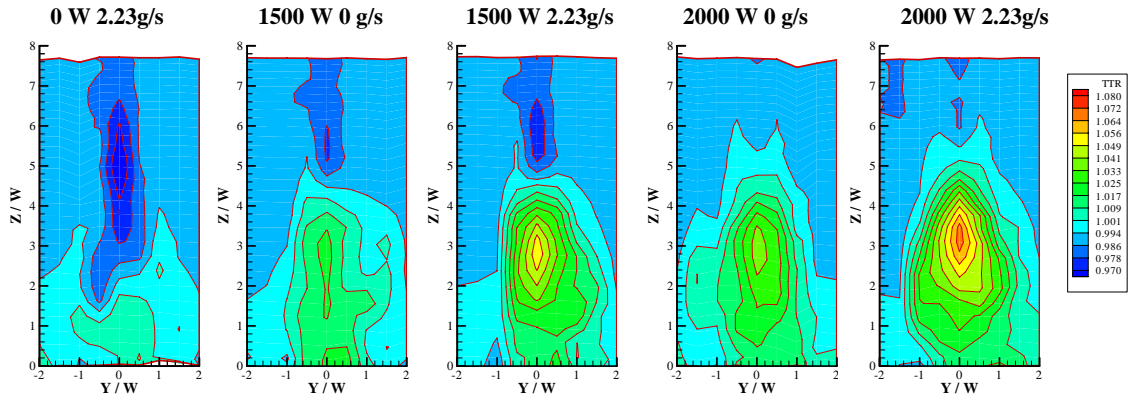
Figure 4-17: Total Temperature Ratio Profiles measured by the thermocouple on the triple probe rake

Figure 4-18 shows the total temperature profile for the two 1500 W plasma torch power tests measured with the total temperature probe (TT) and the triple-probe rake (TP). The difference between the plasma-torch-alone measurements is only about 2%. However the shape of the two profiles differs greatly. The measurements with the fuel show a similar shape, but differ in measured value by 9%.
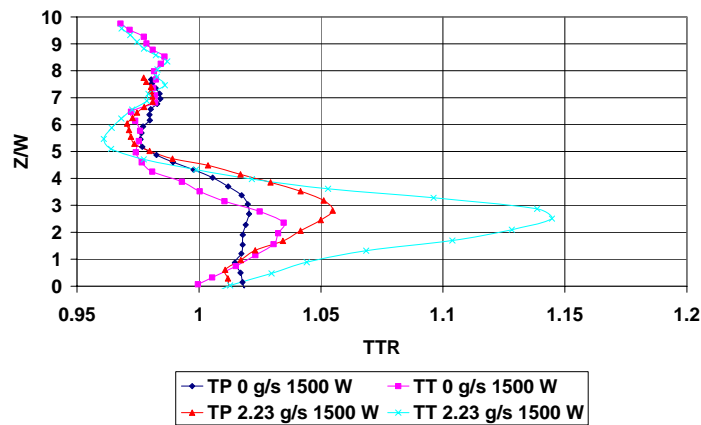
Figure 4-18: Total temperature ratio comparison for measurements made with Total Temperature rake (TT) and Triple Probe rake (TP) for P = 1500 W at the same location

Figure 4-19 shows the total temperature ratio comparison for the test with 2000 W to the plasma torch. In this case, the difference in the measured total temperature ratio for the no fuel- and fuel-on cases were 3% and 10% respectively. Also, the profiles for

55

the triple-probe rake measurement show the temperature rise occurring higher (at a larger Z/W) in the flow than the total temperature probe measurements.
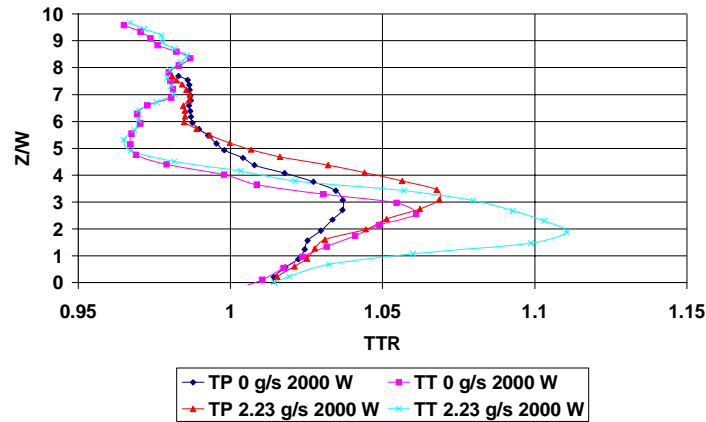
Figure 4-19: Total temperature ratio comparison for measurements made with Total Temperature rake (TT) and Triple Probe rake (TP) for P = 2000 W at the same location

The differences seen in the measurements done with two different probes and a similar setup could be a difference in the measurement system or a slight difference in the setup. The measurements for the triple-probe are consistently lower than for the total temperature probe. However, the shape of the profile also changed. Therefore, the difference cannot be attributed to a thermocouple that was reading slightly lower than the other. The difference must be due to a subtle change in the setup, either the location of the strut and plasma torch or measurement plane, between the two sets of runs.

Figure 4-20 shows the total pressure ratio, which is the measured total pressure divided by the freestream total pressure. A total pressure loss can be seen in the wake of the strut for all of the tests done. The total pressure loss increases as the power is increased. Also, the total pressure loss is greater as fuel is injected for a particular power setting on the plasma torch. This is due to the fact that heat release in a supersonic flow causes large total pressure losses. Also, near the floor of the wind tunnel the boundary layer can be seen. At the strut, the boundary layer from the floor merges with the wake of the strut.
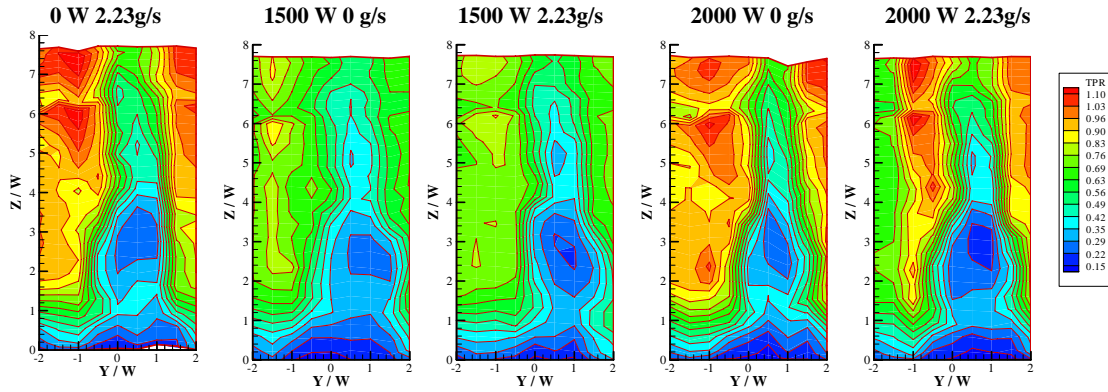
Figure 4-20: Total Pressure Ratio Contours measured by triple-probe rake

Figure 4-21 shows the Mach number contours. The Mach number contours, in general, show the same trends as the total pressure profiles. Far away from the strut, Mach numbers nearing 2.4 are seen, but the flow is not very clean. For the two cases with 1500 W power to the plasma torch, the Mach numbers are lower than for the other cases. Also, the two vertical lines of data on the left of the Configuration B, 2000 W, and 2.23 g/s case are different from the data on the other vertical lines. A possible explanation is that these tests were done on a different day.
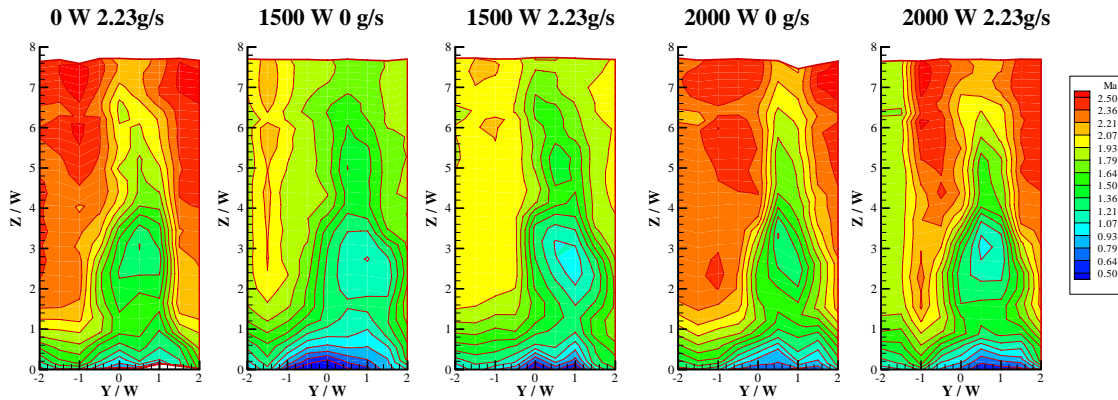
Figure 4-21: Mach Number contours for tests done with triple pressure measurement probe

4.2.2 Total Enthalpy Calculations

The measurements taken with the triple-probe rake allowed the calculation of all of the important properties of the flow. This allowed the amount of energy in the gas in

57

the measurement plane to be calculated. The basic procedure was to calculate the amount of mass flow of gas through a given area. The mass flow of gas was then multiplied by the constant pressure specific heat of air and the total temperature measured at that location. This gives a rough estimate of the total enthalpy of the gas in the measurement plane.

In order to be able to calculate the total enthalpy in the measurement plane, several assumptions had to be made. The first assumption was that the specific heat for all of the gases present was constant with respect to temperature and equal to the value for air. Without this assumption, the calculations of the supersonic properties would have been very difficult. This assumption is a simplification that is the worst possible scenario (yields the lowest estimate of the total enthalpy). The specific heat of ethylene is 54% higher than the specific heat of air. Therefore, any temperature rise of the ethylene would be treated as a temperature rise of the air. Another assumption was that the properties of the flow were locally constant over the area over which they were integrated. A final assumption made was that five of the data points, which had a higher measured cone-static pressures than the measured total pressures were due to a probe interference effect. Because of this probe interference, these points were discarded when the total enthalpy was calculated. These points were generally near the floor of the wind tunnel in the wake of the strut where most of the heat release took place. Therefore, neglecting of these points is again a worst-case scenario.

In order to concentrate on the area where the plasma torch and fuel had the most effect, the total enthalpy was calculated by summing over a portion of the measurement plane. This limited plane is shown in Figure 4-22. By limiting the plane over which the integration was done, the distribution of enthalpy in the areas outside the area of interest did not affect the results.
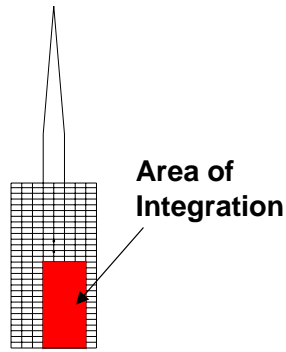
Figure 4-22: Limited area of integration for total enthalpy calculations

Table 4-1 presents the total enthalpy calculated in the measurement plane with the above assumptions. The most obvious trend is that the presence of fuel, and increasing the power to the plasma torch increases the amount of heat release. An interesting result is that for the case with no power and 2.23 g/s of fuel flow rate the total enthalpy is negative. This negative value is due to a drop in the total temperature caused by the wake in a majority of data points in the measurement plane due to the vorticity-induced total temperature drop.

Table 4-1: Total enthalpy in the measurement plane

Power	Fuel	Ho [W]
0	2.23	-268
1500	0	259
1500	2.23	600
2000	0	392
2000	2.23	731

For the 1500W case there appears to be an addition of 260 W, coming from the 1500 W of power supplied to the plasma torch. For the 2000 W case, 392 W of the supplied power is supplied to the flow. These numbers may be a low estimate, because of the fact that the total enthalpy is negative for the case without any power to the plasma torch. This number being negative indicates that there may be more energy being added to the flow than is shown by these numbers. The negative enthalpy value associated with zero torch power should possibly be the reference value.

Table 4-2 presents differences for selected cases of the results presented in Table 4-1. The rows in Table 4-2 are differences between the stated two cases shown in Table 4-1. Looking at the differences between the plasma-torch-alone case and the case with only the fuel and feedstock, more energy is released into the flow than shown by the earlier numbers. This difference is possibly not the best comparison, because fuel is being injected rather than the purge gas, but it is a better indication than the enthalpy rise over the freestream number because the enthalpy rise for the freestream is negative for the case with no plasma torch.

Table 4-2: Total enthalpy difference between different test cases

Case	Difference [W] in Ho
1500W - Fuel and Feedstock	527
2000W - Fuel and Feedstock	660
2000W No Fuel - 1500W No Fuel	133
1500 W Fuel - 1500 W No Fuel	341
2000 W Fuel - 2000 W No Fuel	340

The addition of fuel causes an increase of around 300W for both powers in the measurement plane. This result means that there is little or no benefit in increasing the power to the plasma torch. Comparing the heat release to the higher heating value of ethylene and the mass flow rate of fuel, it appears that the heat release is equivalent to only 0.3% of the fuel burning. With this small amount of heat release it is difficult to say what is happening with the fuel and plasma reaction. There is clearly some type of exothermic reaction taking place, and the amount of reaction increases with the amount of fuel injected. However, it is difficult to speculate on what particular type of reaction is causing the observed heat release.

Chapter 5: Photography and Spectroscopy Results

This chapter presents photographs of test runs and results related to the presence of species that radiate in the plasma or plasma fuel reaction zone. The presence of species is studied qualitatively using filtered photography and quantitatively using the spectrometer. The first section in this chapter presents images of the plasma, and plasma fuel interaction. The second section presents the spectrometer results.

5.1 Filtered Photography Results

Filtered photographs were taken of all runs. During a run a single filter was used with different exposure times to get the best possible picture. During developing, the prints were adjusted to give the best possible contrast and color. However, this development procedure led to slight differences in the brightness of the pictures, and variations in the position of the strut and plasma torch for pictures of different runs. These inconsistencies aside, these pictures remain a useful tool to see qualitatively what is happening with the fuel-plasma torch interaction. None of the Configuration C pictures could be used because there was not enough light to produce a well-developed picture. The pictures shown in Figure 5-1 were taken of Configuration B without a filter. These pictures help to give a visual idea of what the plasma torch alone and the plasma torch-fuel interaction looks like. The figure shows the plasma torch operating at 1500 W power with no fuel and with fuel. In the case with no fuel flow, the most interesting feature of the picture is the brown plume extending downstream from the plasma torch. This plume is associated with NO_2, and its presence means that the nitrogen plasma is reacting with the surrounding air to create NO. This NO then reacts with oxygen to create NO_2. Once the fuel is turned on, even at the lowest flow rate of fuel tested, this plume disappears.

The area of bright light emission also increases, showing that there is some reaction occurring with the fuel. From these pictures the reaction zone is seen as an area, when it is actually a volume. However, with the pictures taken it is not possible to know the spanwise extent of the reaction. From the enthalpy calculations presented in the last chapter, this area of reaction is not due to complete burning of the fuel, but must be associated with the breaking down of the fuel. The location of the top fuel injection hole is indicated in this picture, and the area of reaction does not extend all the way to the top fuel injection hole. This result, as discussed in the previous chapter, is likely due to the fuel injection from the bottom holes blocking the plasma from reacting with the fuel from the higher fuel injection holes.

No Fuel   **0.651 g/s Fuel**
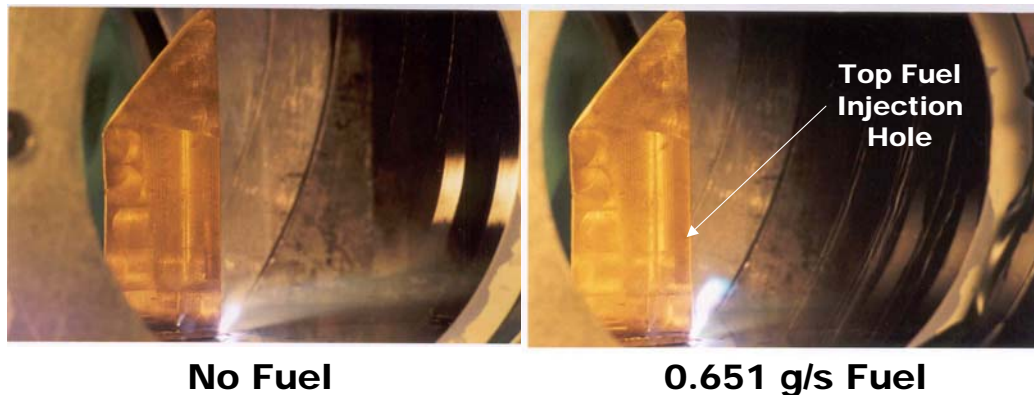
Figure 5-1: Photograph of strut and plasma torch with no fuel and fuel

Figure 5-2 shows pictures of the plasma fuel interaction for Configuration A with varying mass flow rates of fuel. These pictures were taken with shorter exposure time to better show the shape of the area of reaction. As expected, the area of reaction increases with the amount of fuel injected. However, the area of reaction has an unusual shape. The area of reaction is above the plasma torch and has a finger-like region extending from the strut. The fuel and plasma are not reacting near the plasma torch, and the reaction is taking place in a small area. This result led to the creation of Configuration B with the fuel injection holes closest to the floor of the wind tunnel enlarged to increase the fuel flow near the plasma torch.
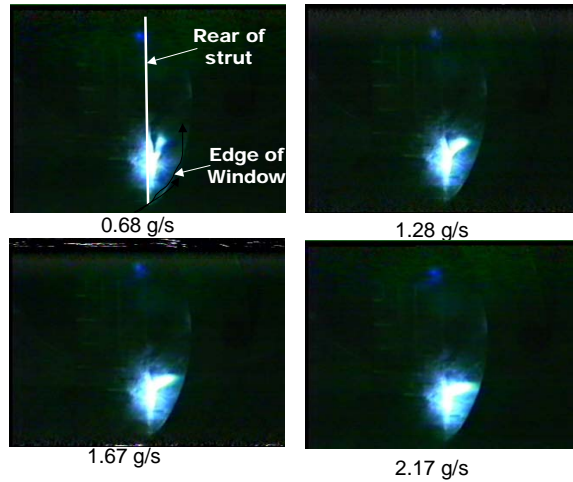
Figure 5-2: Photographs of the plasma-fuel reaction area for Configuration A with P = 1500 and varying fuel flow rates (Brightness of pictures lowered to accentuate the area of reaction)

The areas of reaction for Configuration B are shown in Figure 5-3. The changes made to create configuration B had the desired result, namely the area of reaction moved closer to the wind tunnel floor. However, the majority of the reaction still occurs well above the floor and away from the strut. These observations of the shape of the area of reaction indicate that the plasma torch continues to block the bottom fuel injectors. Also, these pictures show that the fuel and the plasma need some time to mix before they react.
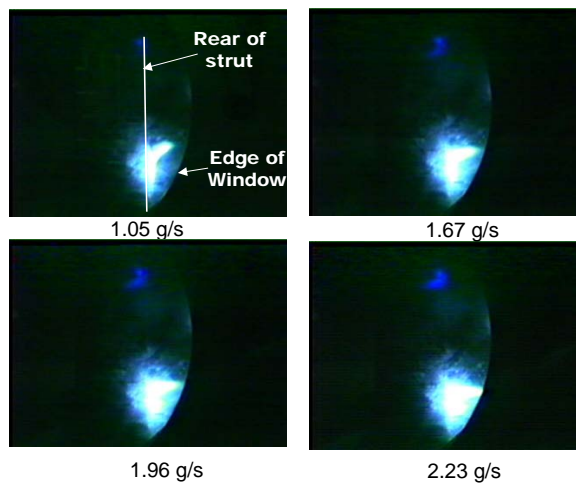
Figure 5-3: Photographs of the plasma-fuel reaction area for Configuration B with P = 1500 W and varying fuel flow rates (Brightness of pictures lowered to accentuate the area of reaction)

63

Figure 5-4 shows the effect of power on the areas of reaction seen. The increase in power from 1500 to 2000 W does not appear to have a large effect on the area of reaction. The area of reaction appears to be brighter, but the increase is small. This result indicates that there is little additional reaction caused by the increase in power, and it could mean the temperature rise seen with the increased power was due to the energy added to the flow by the torch.
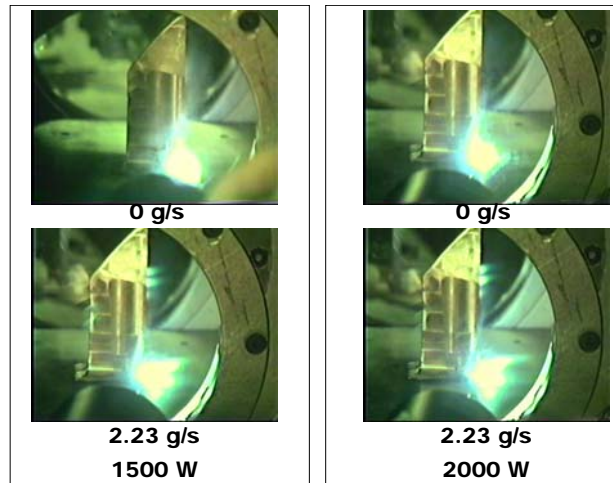
Figure 5-4: Photographs of strut and plasma torch for the same fuel flow rates and varying powers

Figure 5-5 shows the pictures for Configuration C with the strut moved 2 strut-widths upstream of the plasma torch. These pictures present the best evidence of the strong effect that the torch has as a flameholder. Here, the only role the strut plays is to inject the fuel out into the flow. The plasma torch then causes the reaction of the fuel near where the plasma is injected. The effect of the plasma torch is diluted because there is less of a wake from the strut in which the reaction can take place. This dilution causes the smaller temperature rise for Configuration C than for Configurations A and B. This dilution can also be seen by comparing the 0 g/s (no fuel) cases for Configuration C shown in Figure 5-5 with Configuration B shown in Figure 5-4. This increase in dilution for the the Configuration C case causes a more prominent plume of NO_2 than in the Configuration B cases.
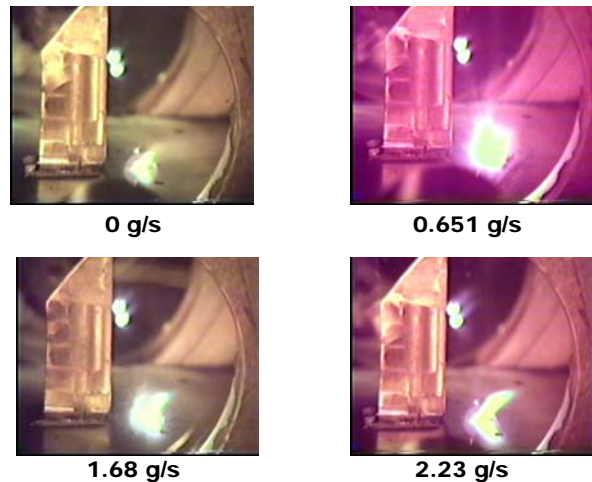
Figure 5-5: Photographs of strut and plasma torch for Configuration C with P = 1500 W and varying fuel flow rates

Several filters were also used to get a qualitative view of the intensity and types of species present. The first filter used had a center wavelength of 310nm and transmitted wavelengths ± 10nm from this point. The purpose of this filter was to isolate the light associated with the OH* radical. However, as stated in the previous chapter, not much of the fuel actually burned during these tests so there would be little OH* present. However, because of the bandwidth of the filter there was some other light transmitted through the filter. The 310nm filter would also pick up some of the stronger CN lines. It is not until the spectrometer results are examined in the next section that the source of this light can be definitely stated.

Figure 5-6 shows the 310nm-filtered photographs for Configuration B with 1500 W plasma torch power. Some light in this wavelength range is seen even for the case with the plasma torch only. This result could be due to the presence of some excited nitrogen spectral lines in this wavelength region, or simply from the plasma torch giving off some broadband light. As the fuel flow rate is increased, the brightest area moves out away from the torch and becomes much wider. This widening of the intense area indicates that more of the fuel is reacting with the plasma.

0 g/s	0.651 g/s
1.68 g/s	2.23 g/s
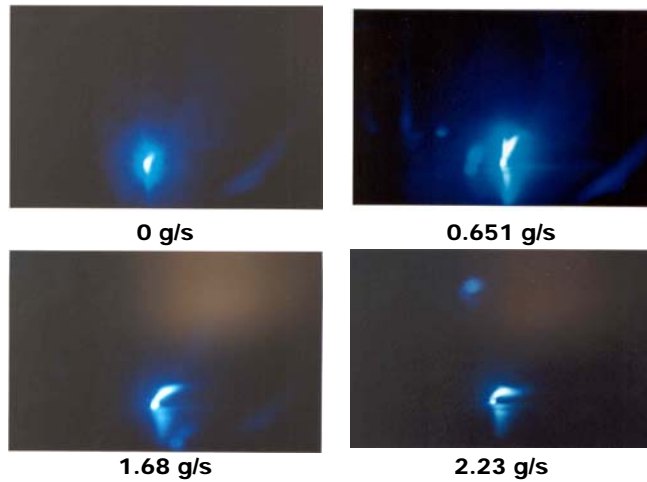
Figure 5-6: 310nm filtered photographs of Configuration B with P = 1500 W and varying fuel flow rates

Figure 5-7 shows the 310nm-filtered photographs for the three powers tested at 2.23 g/s of fuel flow. These pictures show little difference as the power is increased. The 2000 W and 2500 W pictures appear to have a somewhat larger area of reaction, but the difference is not considered to be significant . This result is another indication that torch power does not strongly affect the results.

1500 W   **2000 W**   **2500 W**
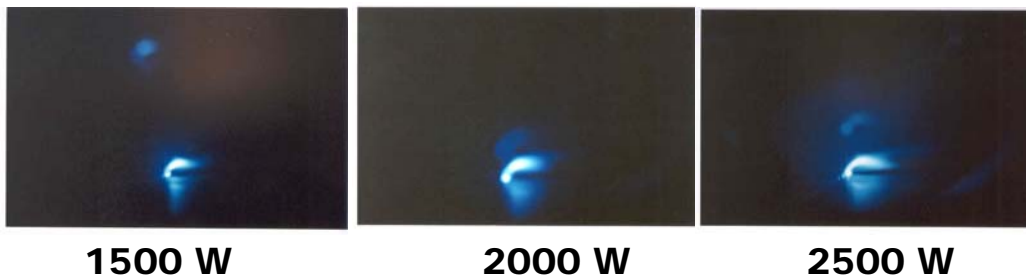
Figure 5-7: Comparison of 310nm filtered photographs of Configuration B with a fuel flow rate of 2.23 g/s and varying powers

The next filter used had a 515nm center wavelength and allowed wavelengths of ±9nm from this point to pass through. This filter targeted wavelengths associated with the C_2^* Swan system. The filter did not transmit enough light without fuel flow to expose the film. Therefore, the light seen through these filters, shown in Figure 5-8, is caused by the fuel-plasma torch interaction. As the amount of fuel increased, so did the area of

66

fuel-plasma interaction. The shape of the area of reaction also changed. With the smallest fuel flow the area of reaction was more erect. As the fuel flow rate was increased the area of reaction moved away from the strut. These pictures show similar results to the regular photographs of the area of reaction and those with the 310nm filter.

| 0.651 g/s | 1.68 g/s | 2.23 g/s |
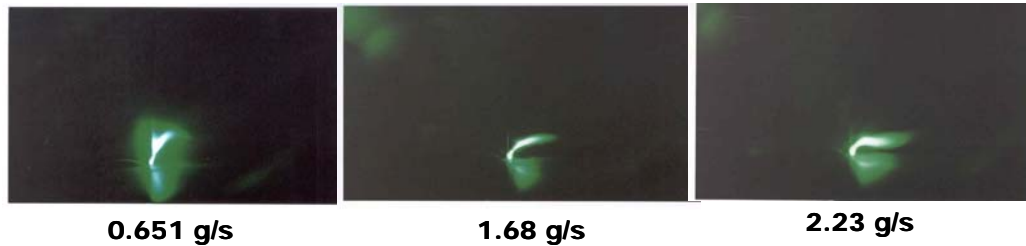
Figure 5-8: 515nm-filtered photographs of Configuration B with P = 1500 W and varying fuel flow rates

Figure 5-9 shows the 515nm filtered photographs for 2.23 g/s of fuel flow at all of the powers tested. Again, there is little change in the shape, size, or intensity of the area of reaction for all of the powers tested. Increasing the power increases the intensity in the photograph slightly. Also the shapes for all powers are very similar. There is little evidence that increasing the power changes the types of species present noticeably.

| 1500 W | 2000 W | 2500 W |
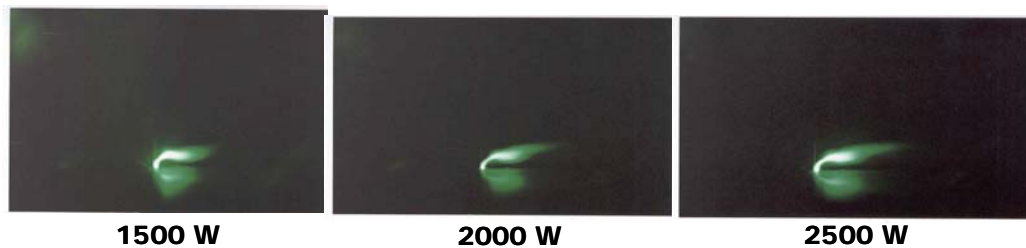
Figure 5-9: 515nm-filtered photographs of Configuration B with a fuel flow rate of 2.23 g/s and varying powers

The 656nm filter was meant to transmit light associated with the H_α line of the Balmer series. This filter had a wavelength spread of 11nm, and in that wavelength region there is also a CN line. The photographs using this filter are shown in Figure 5-10. There is some light transferred through with no fuel injection. The source of this light is likely the white light from the plasma torch including some light over all

wavelengths. Also, the filter is more transparent than the other filters, as can be seen by the strut being visible in the pictures. The area of visible reaction increases with the amount of fuel injected, as it has for all of the filters. Also, the shape changes as in the earlier photographs.
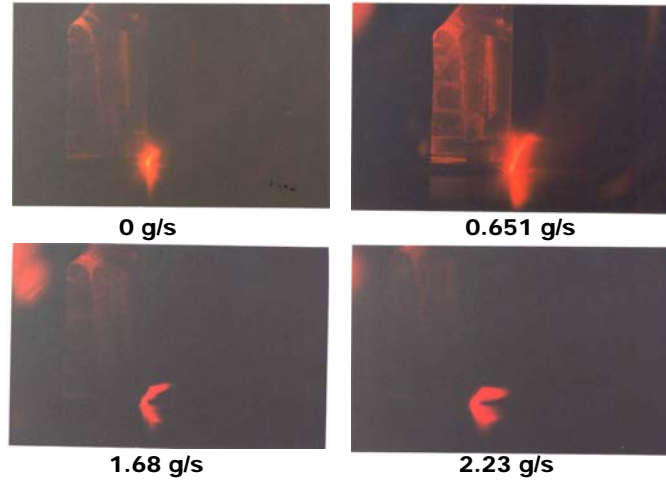
Figure 5-10: 656nm-filtered photographs of Configuration B with P = 1500 W and varying fuel flow rates

The 431nm filter was meant to capture light associated with CH^*. The filter allowed wavelengths within ±8nm of 431nm through, which would also include several of the CH^* lines as well as some excited nitrogen lines. However, the only pictures that were bright enough for printing were for the maximum fuel flow rate of 2.23 g/s. These pictures are shown in Figure 5-11. Again, in these pictures little difference is seen in the area of reaction. The overall intensity of the picture does vary, with the 2000 W case being the brightest, but this difference could be caused by the development process.
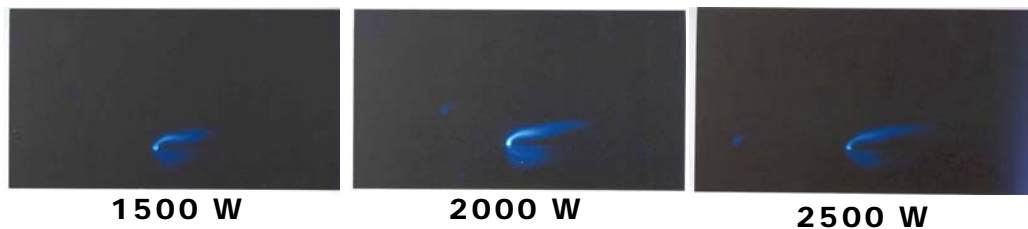
Figure 5-11: 431nm-filtered photographs with a fuel flow rate of 2.23 g/s of fuel and varying powers

5.2 Spectroscopy Results

During the testing of Configurations B and C, spectrometer data was acquired. The spectrometer data was taken in a rectangular grid of points, but only the points of most interest will be discussed in the next section. In the second section, contour plots of selected species will be presented. For all the data, unless noted otherwise, two samples with a 100 ms integration time were averaged. The integration time is the time that the spectrometer collects photons for a sample, and it was adjusted to give the best intensity for the brightest cases without saturating the output of the spectrometer. The samples were averaged to reduce the noise of the low intensity wavelengths. The samples averaged together with the integration time meant that data was taken over a number of torch cycles as was discussed in Chapter 2.

5.2.1 Whole Spectrogram results

This section presents the intensities measured over the entire wavelength range of the spectrometer used. The spectrometer had three channels, each covering a band of wavelengths, namely 195-410 nm, 395-625nm, and 550–800nm. The fiber optic cable to one of these channels was broken so the highest wavelength band was not used. Also, no significant peaks were seen below 250 nm. Therefore, the plots shown are limited to a range of 250 nm to 625 nm. First, plots analyzing the plasma alone are shown. Then, plots showing the plasma-fuel interaction are given.

Figure 5-12 shows a plot of the spectrum measured near the plasma torch exit. Most of the peaks seen are associated with the 2nd N_2 positive system and will be discussed more in the next paragraph. The plot shows a strong decrease in the intensity with an increase in the vertical distance from the torch exit. The same peaks appear to be prominent at all positions. So, there does not appear to be significant change in the makeup of the excited species present.
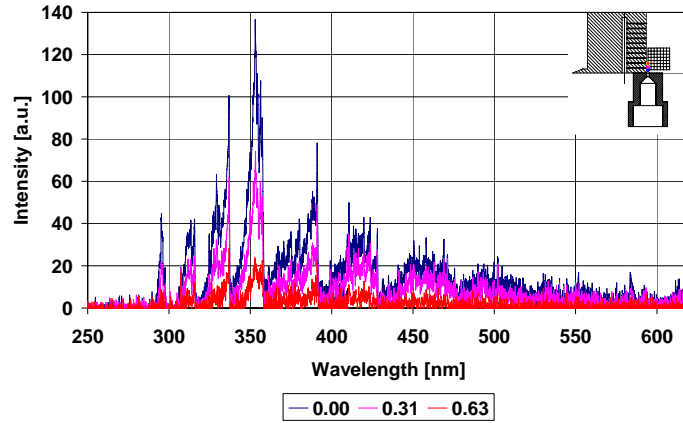
Figure 5-12: Spectrogram of plasma torch only for P = 1500 W and X/W = 0 and different Z/W positions

Figure 5-13 shows the same spectrogram in the 280nm to 360nm range. The most prominent peaks are labeled, and all of the peaks are associated with the 2nd positive N_2 system. The peaks in this region could be caused by the presence of other species, but it is unlikely because so many of the peaks are present. Also, all of the peaks appear degraded to violet. This degradation is consistent with the 2nd N_2 positive system.
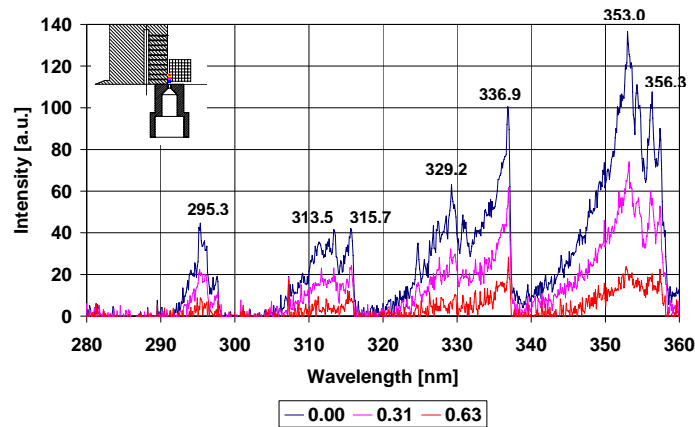
Figure 5-13: Spectrogram of the 280-360 nm range for P = 1500W, X/W = 0 and varying Z/W

The spectrograms for the plasma torch alone with powers of 1500W and 2000W are shown in Figure 5-14. Most of the peaks present in the 1500W spectrum are present in the 2000W spectrum. However, the 2000W spectrum has a number of strong peaks

not present in the 1500 W spectrum. The 600.8nm and 403.5 nm peaks are most likely lines associated with NO. The 403.5nm peak appears to be associated with the NO β system. However, none of the other prominent peaks are observed. Most of these peaks occur near other peaks that are stronger.   The 446.3nm peak is most likely caused by the presence of tungsten oxide. The cathode of the plasma torch was made of tungsten, and at higher powers more electrode erosion occurs. Small particles of the cathode are regularly ejected into the flow. The other peaks at 510.0nm, 466.7nm, and 468.0nm were not identified. These strong peaks occur only at high powers and could not be associated with the nitrogen feedstock, air freestream or any of the materials used. Also, Gallimore [2001] and Jacobsen [2001] did not observe these peaks in their earlier work. These peaks may be associated with the copper and tin that are present in the brass, which is the material of the strut. Gallimore and Jacobsen would not have had these elements present.
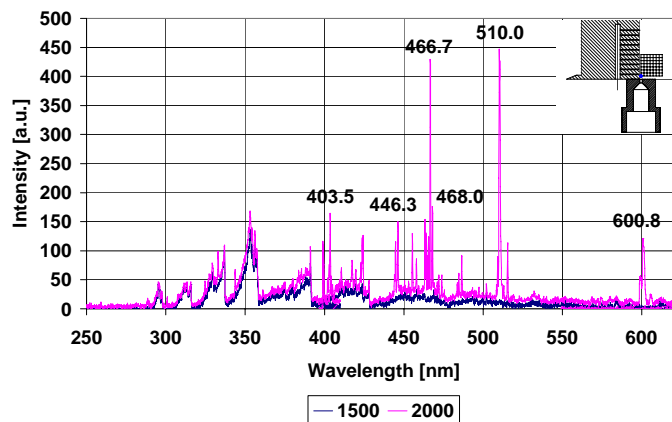
Figure 5-14: Spectrogram Comparing P = 1500W and P = 2000W at X/W = 0, Z/W = 0 with peaks that differed labeled

Figure 5-15 shows the effect of adding fuel to the flow with the same power at a location near the plasma torch. The spectrogram shows that the N_2 positive system lines are as strong with the fuel addition as without the fuel. However, a new system of lines associated with CN appears. These two results together are interesting. Even though some of the active nitrogen is reacting with the fuel, there appears to be little reduction of the active nitrogen lines. This apparent inconsistency is most likely caused by a difference in the intensity of the lines emitted by these species.
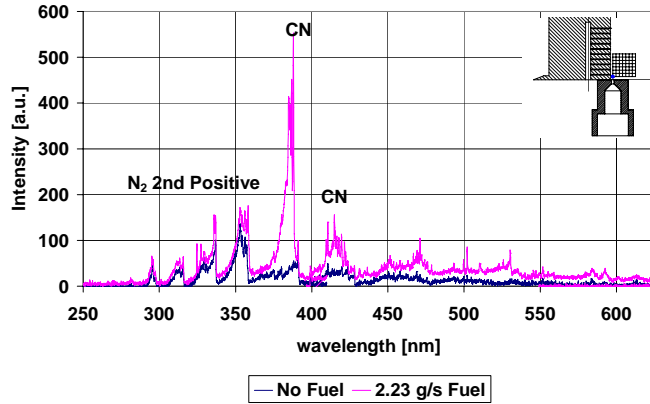
Figure 5-15: Spectrogram of fuel and no fuel cases at X/W = 0, Y/W = 0 and P = 1500W

Figure 5-16 shows the spectrogram with and without fuel farther away from the plasma torch. The spectrogram for the fuel and no-fuel cases farther from the plasma torch show that the prominent species are completely different. At this location, the active nitrogen species are no longer present, while the CN lines are the dominant feature. Also the C_2 Swan system that is barely visible in Figure 5-15 above is now more defined.
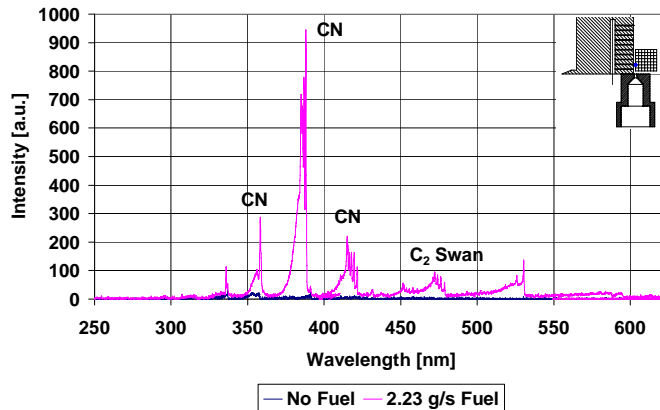
Figure 5-16: Spectrogram for fuel and no fuel at X/W = 0 and Z/W = 0.63 and with P = 1500 W

Figure 5-17 shows the spectrograms for 1500 W power to the plasma torch and varying mass flow rates of fuel. From the figure it is apparent that even a small amount of fuel causes a large amount of CN to be present. The amount of CN and C_2 seen also increases as the mass flow rate of fuel is increased. There is no real change in the types of species seen as the mass flow rate of fuel is increased. Only the intensity changes as

the amount of fuel increases. Therefore, the increase in mass flow rate of fuel must be causing more of the fuel to mix with the active nitrogen to produce the change in intensity, and is not changing the types of species present.
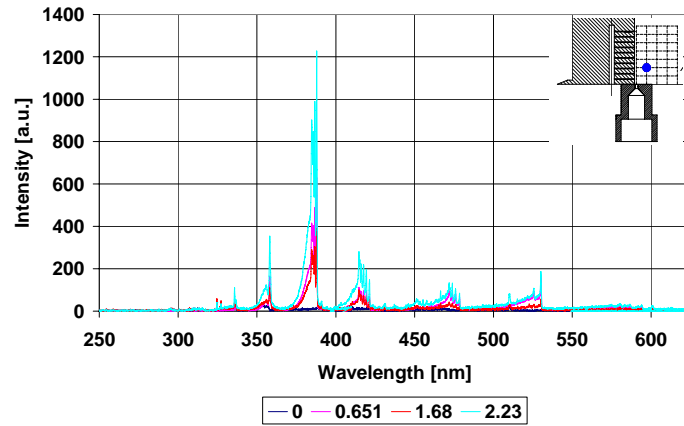
Figure 5-17: Spectrograms for varying fuel flow rates with P = 1500 W at X/W = 0.98 and Y/W =1.57

Figure 5-18 shows the spectrogram for varying torch powers and the same mass flow rate of fuel. Increasing the torch power does not have a strong effect on the types and intensities of the species present. This result lends further evidence to the conclusion that the power to the plasma torch has little effect on the chemistry of what is happening in the fuel plasma interaction. The additional temperature rise observed with the higher powers comes purely from the extra energy in the plasma and not because of any increased reaction of the fuel with the plasma.
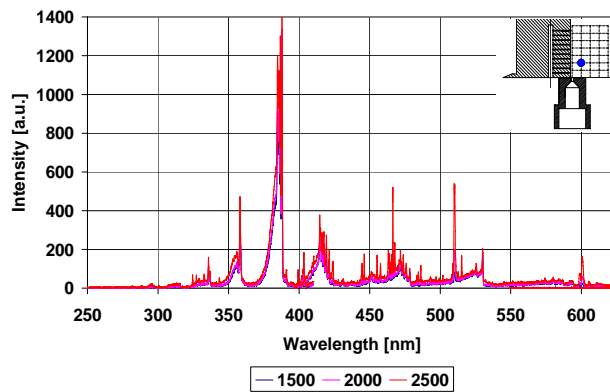
Figure 5-18: Spectrograms for varying powers with fuel flow rate of 2.23 g/s, at X/W = 0.98 and Z/W = 1.57

5.2.2 Excited Species Contour Plots

Contour plots were made for all runs for a range of wavelengths that contained excited species of interest. Figure 5-19 shows the contour plots for CN for Configuration B with a power of 1500 W. The range for this plot, as well as for the rest of the contour plots, is plotted with an exponential distribution. An exponential distribution was used because there was a large difference between the lowest intensity seen and the highest. Also, the maximum intensity seen could increase greatly between different cases. As the mass flow rate of fuel is increased, there is not much change in intensity of CN. The lowest intensity occurs for the middle flow rate of fuel. Also, the height at which the maximum intensity occurs moves downward as the fuel mass flow rate is increased. This result is consistent with the results shown in the last chapter. The reaction taking place occurs at or near a single point, and the area of reaction then spreads outward from that single point.
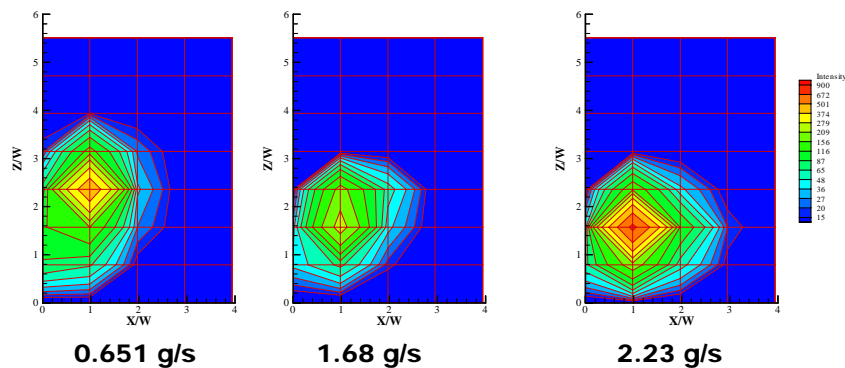
Figure 5-19: Contour plot of CN for Configuration B with a power of 1500W and varying fuel flow rates

Figure 5-20 shows the contour plots for 2.23 g/s of fuel and varying powers. There is not much difference in both the maximum intensity and the area of high intensity between the 1500W and 2000W powers. The 2500W case shows a slightly larger area of high intensity and a slightly larger area that has a significant intensity. Here again, we see that power has a small and inconsistent effect on the excited species seen.

1500 W   **2000 W**   **2500 W**
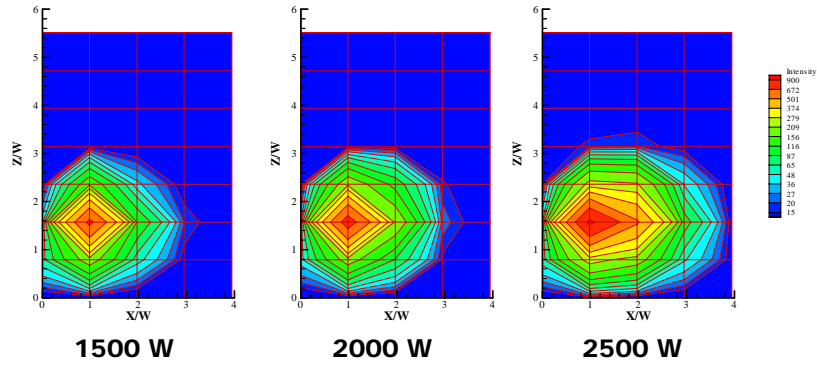
Figure 5-20: Contour plots of CN for Configuration B with fuel flow rate of 2.23 g/s and varying powers

Figure 5-21 shows contour plots for the C_2 lines for Configuration B with 1500W of power and varying mass flow rates of fuel. Again, the 1.68 g/s fuel flow rate case has the lowest intensity. The lowest fuel flow rate case has the most elevated area of reaction. Also, the area of reaction does not seen to be centered on a single point as for the CN case. The area of reaction comes from the plasma torch, which is closer to the floor of the wind tunnel.

0.651 g/s   **1.68 g/s**   **2.23 g/s**
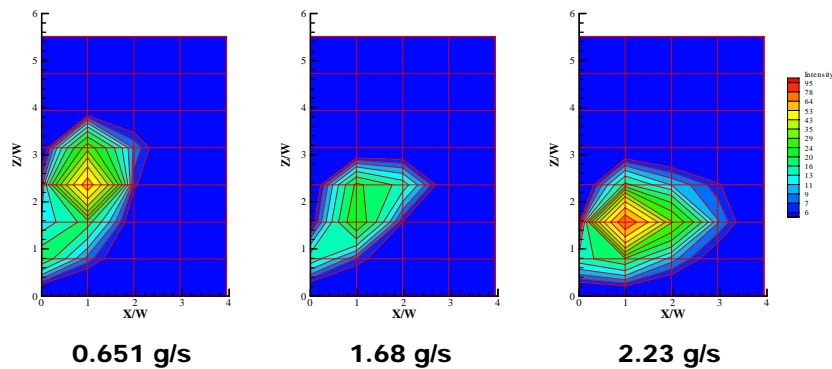
Figure 5-21: C_2 contour plots for Configuration B with P = 1500 W power and varying fuel flow rates

Figure 5-22 shows the C_2 contour plots for Configuration B with 2.23 g/s of fuel and varying power. All of the plots have the same shape for the area of reaction with a difference in the maximum intensity seen. Here, the power seems to have a stronger effect on the intensities seen. However, the overall intensities seen for C_2 are small compared to the intensities seen for CN.

75
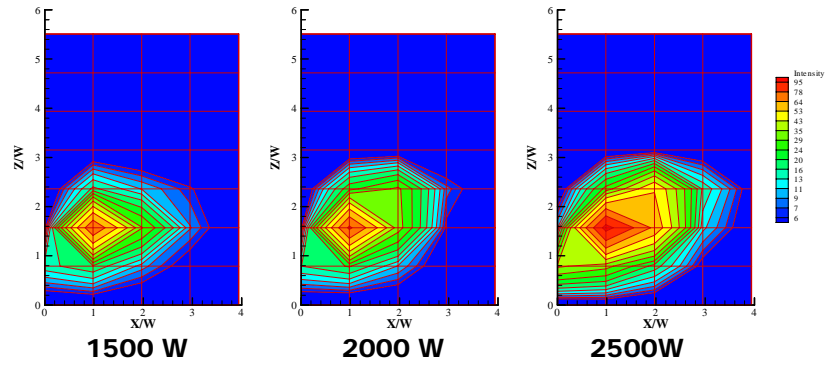
Figure 5-22: C$_2$ contour plots for Configuration B with fuel flow rate of 2.23g/s and varying powers

Chapter 6: Conclusions and Recommendations

This chapter serves to summarize all of the work done in the current study, and present the most important conclusions of this study. Also, some recommendations will be made for future work in this area.

6.1 Summary and Conclusions

In this study, a fuel injection strut was tested in conjunction with a plasma torch as an igniter-flameholder combination. Both aerothermodynamic and spectroscopic data were taken and analyzed. Three configurations were tested. Two of the configurations, Configurations A and B, had the plasma torch mounted just behind the base of the strut. Configuration A had all ten of the fuel injection holes the same size. The bottom four holes were enlarged, defining Configuration B. Configuration C was produced by taking the strut as it was setup for Configuration B, and moving it two strut-widths upstream.

From these data, several conclusions can be drawn. The first conclusion is that there was some type of exothermic reaction taking place. However, the spectroscopic and total enthalpy calculations have shown that little of the fuel is being completely burned. The enthalpy calculations showed that on the order of 0.3% of the fuel is being burned. The spectroscopic results showed that there are no OH^* radicals present, which is usually the dominant feature of a combustion spectrum.

The exact source of the heat release is difficult to identify, but it was definitely caused by the fuel-plasma interaction. The most dominant lines of the fuel and plasma spectrum were the lines associated with CN and C_2. Therefore, the plasma was breaking down the fuel, but little was seen of the hydrogen associated with the fuel. Little CH^*

77

was seen, and the dominant H[*] lines were in the region of wavelengths that could not be surveyed.

Also, as the amount of fuel was increased, the amount of reaction between the fuel and the plasma increased. The measured temperature results show more heat release as the mass flow rate of fuel increased. The spectrometer results also showed more excited fuel-plasma related species present as the mass flow rate of fuel was increased. Therefore, the plasma present was able to react with more fuel, so the plasma was not the limiting agent in the reaction.

The second conclusion that can be drawn is that Configuration C performed the best at allowing the plasma torch to penetrate out into the flow. However, the overall temperature rise seen was less for Configuration C than for the other configurations. This difference was likely caused by the fact that the plasma torch had to act as the flameholder rather than the strut. Therefore, the strut served only as means of injecting the fuel out into the flow. Also, the fuel injectors were far enough away from the plasma torch to prevent the fuel flow coming from the lower injectors from blocking the plasma reaction with the fuel flow from the upper injectors.

The pattern of temperature rise showed more heat release near the middle injectors and, for the most part, off of the centerline. This pattern is believed to be caused by the fuel injection and plasma torch interacting. The injection from the plasma torch acts as a blockage to the bottom fuel injection holes, and this blockage forces more of the fuel through the middle and top injectors. The change to Configuration B increased the heat release at the lower injectors some, but the majority of the heat release remained well above the floor.

The fuel and plasma together also caused the temperature rise to take place off the centerline of the strut. The plasma injected from the bottom tended to hit the fuel from the fuel injectors, causing the fuel to turn to the right, when looking upstream, and the plasma to turn slightly to the left. This interaction can be most clearly seen in the total temperature surveys with and without the purge and feedstock supply.

The fuel and plasma interaction also caused the reduced penetration height of Configurations A and B as was discussed above. The fuel injected from the middle injectors blocked the plasma from the fuel from the higher injectors.

78

The change in the fuel injection hole pattern helped to increase the amount of heat release seen near the floor of the wind tunnel. However, the heat release remained well above the floor. This result was explained earlier by the fuel plasma torch interaction. Increasing the hole-size of the lower injectors had some effect on the results. The heat release did move a little closer to the floor of the wind tunnel, and the maximum temperature rise increased. The maximum temperature rise increased because more of the fuel was forced out of the lower holes and into the plasma.

Finally, the power to the plasma torch had, at best, an inconsistent effect on the amount of reaction seen. Both the total enthalpy and spectroscopic results showed little increased reaction when the power was increased. The temperature rise increased but this was caused by the increase in the amount of energy that the plasma transferred to the flow. The total enthalpy calculations showed that there was the same amount of heat release when fuel was injected compared to when it was not, for both powers tested. Also, the spectroscopic results showed little change in both the intensity and types of species present.

This inconsistent effect of the power is difficult to explain with any certainty. Either the process going on in the torch changes as the power to the torch is changed, or the plasma present is sufficient to react to the extent that the reaction will take place with the amount of fuel that is present. The combination of the result of having the amount of heat release increase with the fuel flow rate and having the same total enthalpy rise over the plasma torch alone for the different power levels, indicates that the amount of plasma present is sufficient for the mass flow rate of fuel present. The addition of more excited species, produced with a higher power, causes no more reaction to take place because the rate of reaction of the fuel is the limiting reactant. The cold environment in the supersonic tunnel probably contributed to this result.

An interesting phenomenon occurred during a wind tunnel run in which the fuel line was being purged with the plasma torch on. The plasma-fuel reaction area behaved as shown in Chapter 5, but as the fuel line was emptied the plume started to extend up the entire length of the strut. A photo of this phenomenon occurring is shown in Figure 6-1. It is not known exactly what caused this spreading of the plasma plume, but repeating the purging procedure reproduced the spreading effect. A possible explanation of this

behavior could be that without the fuel or the purge to block the plasma, it was able to travel farther up the back of the strut. However, runs without any injection through the strut were unsuccessful in repeating this result. It seems that the transient nature of the purging procedure was important.
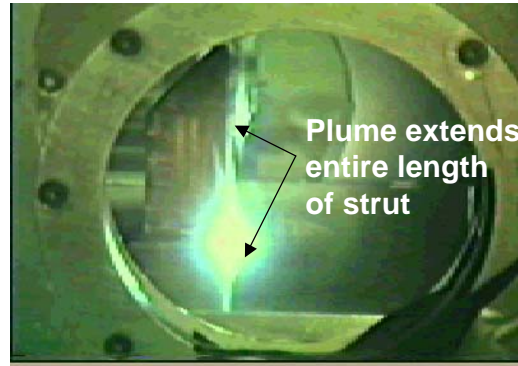
Figure 6-1: Photograph of plume extending the entire length of the strut

6.2 Recommendations for Future Work

Based on the conclusions of the present work and the overall direction of Scramjet research in general, several recommendations can be made for future work. The first recommendation would be to further investigate the plume extending up the back of the strut as discussed above. This effect is not well understood, and could not be reproduced consistently. A more in-depth investigation of this phenomenon could lead to a way to effectively spread the plasma from its single point of origin across an engine. This spreading would help to eliminate the need for multiple plasma torches in an engine flow path.

The second recommendation is to investigate the lateral spreading of the effects of the fuel-plasma torch interaction. An understanding of the spanwise spreading would, again, help to eliminate the need for multiple plasma torches in the engine. Some idea of the lateral spreading could be gathered from the total temperature and triple probe rake measurements. However, a spectroscopic investigation of the spreading would be beneficial. Mounting the strut and the plasma torch in the door of the wind tunnel and

taking measurements through the window in the other door would be one way to accomplish this set of tests.

Testing needs to be done with the plasma torch and a more realistic strut geometry than was used in this study. The strut used was designed to investigate burning in a wake region, it was not meant to be representative of a combustion strut. A more realistic strut, tested with realistic mass flow rates of fuel, and in a heated wind tunnel would greatly increase the understanding of the plasma-fuel interaction.

Testing needs to be done with heavier hydrocarbons as fuels. As technology makes Scramjet engines more feasible, producing large amounts of thrust with a reasonable fuel volume and practical operating ranges will make the use of liquid hydrocarbon fuels necessary. Liquid hydrocarbon fuels are easier to store and have a higher energy density than gaseous hydrogen. However, liquid hydrocarbons are more difficult to burn because of their more complicated composition. Recently, the trend is to use the liquid fuel as a coolant for the airframe of the aircraft. In flight, the fuel is heated to such a degree that the fuel is cracked into simpler components. The simpler components are easier to burn, but produce a new set of challenges. A plasma torch needs to be tested with these fuels, including cracked compositions, to see how well it will perform as an igniter and flameholder.

Appemdix A: Development of the Virginia Tech Plasma Torch

Wagner [1987] was the first Virginia Tech researcher to use a plasma torch in a supersonic combustion application. Two plasma torches were used in his study. The first was a commercial plasma torch from Plasmadyne, shown in Figure A-1. This torch was water cooled, and could be operated on powers levels up to 80 kW. A tangential gas inlet was used to introduce a swirl to the feedstock flow, which increased the electrode lifetime. The torch was designed to use argon, hydrogen, nitrogen, or mixtures of argon with either nitrogen or hydrogen. However, hydrogen was the main feedstock used. The torch was designed to be water cooled to keep the temperature of the torch down. The Plasmadyne torch did not perform well in the supersonic combustion tests. The main reason for this poor performance was that the exit of the torch was not choked. Since the exit of the torch was not choked, any pressure fluctuations at the outlet of the torch could affect the stability of the operation of the torch. These pressure fluctuations could be caused by changing conditions in the wind tunnel or by the changes caused by ignition of the fuel. Because the goal of the torch was to ignite the fuel and because this ignition could cause the torch to go out, a new torch was needed.
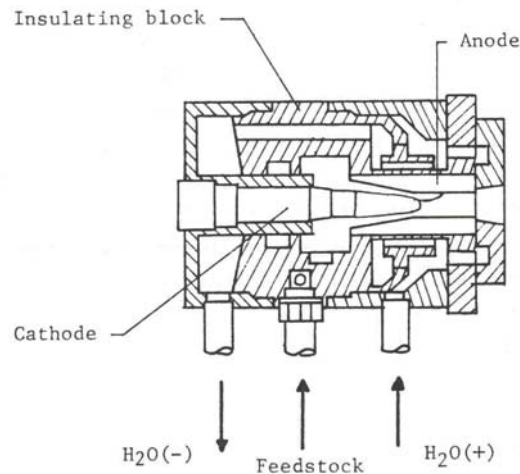
Figure A-1: Section drawing of the Plasmadyne torch adapted from Wagner [1987]

Barbi [1986] developed a torch to address the problem of an unchoked exit. Figure A-2 shows a section drawing of the first generation Virginia Tech Plasma Torch. This torch was designed to have a choked exit and to operate on relatively low powers of around 1 kW. Like the Plasmadyne torch, a tangential inlet for the feedstock gas was also used to move the attachment point of the arc. Because the torch was also designed to be uncooled, the heat normally carried away by the cooling water was added to the flow. Because the energy previously carried away by the cooling water was now added to the supersonic flow, this plasma torch was more efficient.
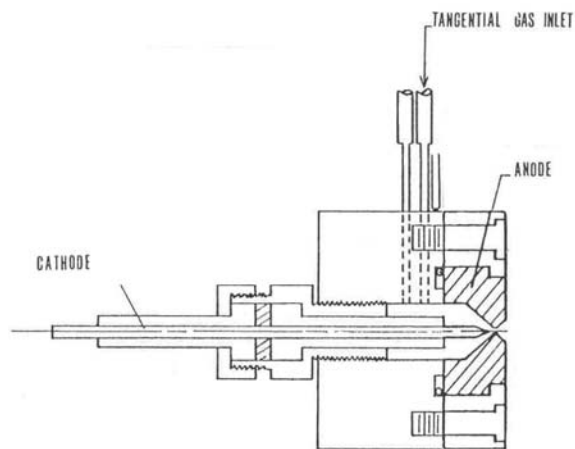
Figure A-2: Section drawing of the plasma torch developed adapted from Barbi [1986]

Barbi tested the torch on powers of 0.5 to 2 kW. The torch was also able to run on a wide range of mixtures of hydrogen and argon as the feedstock. The power required to maintain a constant current increased linearly with the amount of hydrogen and a constant amount of argon in the feedstock. The thermal efficiency, defined as the ratio of total enthalpy of the gas exiting the torch to the electrical power into the torch, of the torch was found to be 88% by calorimeter tests.

The torch shown in Figure A-3 was developed by Stouffer [1989]. This plasma torch was designed to have a longer electrode lifetime than the first Virginia Tech Plasma Torch. In order to accomplish this increased lifetime, the torch incorporated three main features in the design. The first feature was the addition of a flow swirler to the torch. The flow swirler caused the attachment point of the arc to move around the anode. Since

the arc attachment point was constantly moving around the anode, the arc would not be able to wear the anode at a single point. Therefore the electrodes would last longer.
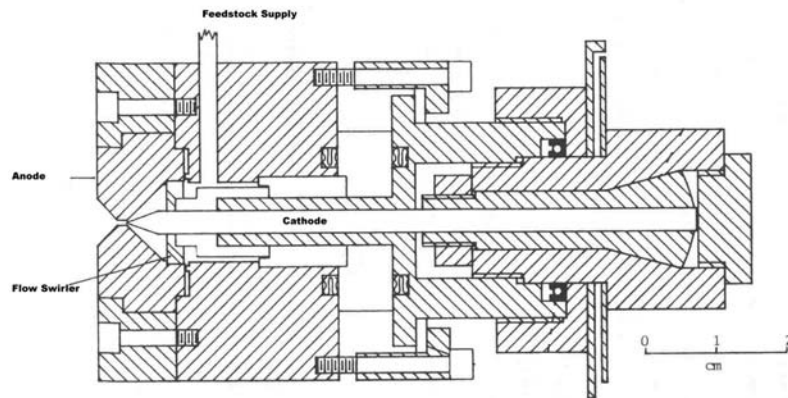
Figure A-3: Section drawing of the torch adapted from Stouffer [1989]

The swirling of the flow also produced additional benefits. By having the swirling of the flow move the arc, a small portion of the feedstock gas stayed in contact with the arc for a relatively long period of time. This increased contact time produced hot pockets of gas that have proved to be more effective at ignition than if the heating by the arc was more evenly distributed. The swirling flow also created a low-pressure area in the constrictor through which the arc could more easily pass. This design helped both to keep the arc away from the walls of the constrictor, and to cool the anode through the constrictor.

The second design feature incorporated into this torch was a better electrode holding system that ensured that the electrodes were aligned. The earlier torch had problems with the arc not traveling through the constrictor and attaching to the inside of the nozzle of the anode. This different attachment point for the arc caused the torch operation to be very unstable. Also, the shorter arc length caused the power of the torch to decrease. Stouffer eliminated this problem by redesigning the body of the torch with an emphasis on alignment of the electrodes.

The third design feature of this torch was that the electrode gap was continuously adjustable. This feature allowed the power output of the torch to be adjusted for any

desired power in the operating range of the torch. Also, as the electrodes wore, the arc gap could be adjusted to give the same power as when the electrodes were new.

Stouffer tested this torch on feedstocks of argon, nitrogen, and mixtures of argon with nitrogen or hydrogen. The stability of the torch was increased to the point that argon no longer needed to be mixed with the desired feedstock gas to obtain stable operation. The lifetime of the electrodes was increased to more than twenty hours when using a mixture of nitrogen and argon as the feedstock.

Gallimore [1998] then tested this torch on various hydrocarbon feedstocks. Gallimore found that the torch did not operate as smoothly on hydrocarbon feedstocks as it did on feedstocks such as nitrogen. Feedstocks such as methane, ethylene, and propane were tested in the torch. The power required for stable operation was found to increase as the molecular weight of the feedstock increased. Gallimore also found that the plasma jet coming from the torch pulsed at a high frequency. This pulsing was caused by AC-power-related variations in the DC power supplied by the arc welders used as a power supply. This pulsing, if it could be controlled, could produce an igniter that could be tuned to the flow.

Gallimore [2001] later developed a torch that was more compact and reliable than the old torch. This torch, shown in Figure A-4, is the one that will be used for the present work, and will be discussed more in the first section of Chapter 3. Gallimore experimented with various shapes for the anode geometry. The final design of the anode (labeled part A) is shown in Figure A-4. This design had an internal geometry that produced the most stable operation, and an exit to the anode that produced the longest-lived excited species. The torch was tested on feedstocks of argon, nitrogen, air, methane, and ethylene. The different feedstocks were evaluated based on the amount and types of ionized species produced. Air and nitrogen were found to be the most effective feedstocks at a given power. Methane and ethylene were less effective. For all subsequent tests, the torch was run on nitrogen, since it proved almost as effective as air and not nearly as erosive to the electrodes.
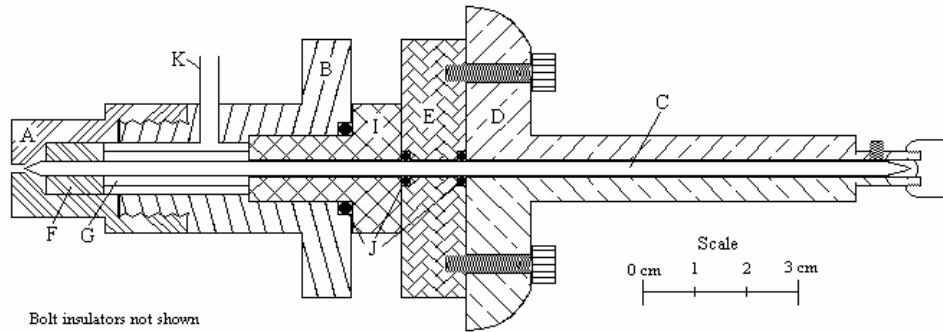
Figure A-4: Section drawing of plasma torch developed by Gallimore [2001]

Another plasma torch was designed based on the design of Gallimore and Jacobsen to be used in a heated supersonic combustion wind tunnel at Wright-Patterson Air Force Base. This torch, shown in Figure A-5, retained all of the major features of the earlier torch, but with a reduced body size. One change made to the torch was the use on an anode insert instead of a one-piece design. The anode inserts were easier and cheaper to manufacture, but were not as robust with respect to the electrode alignment. Wind tunnel testing using this torch has not been conducted as of this writing.
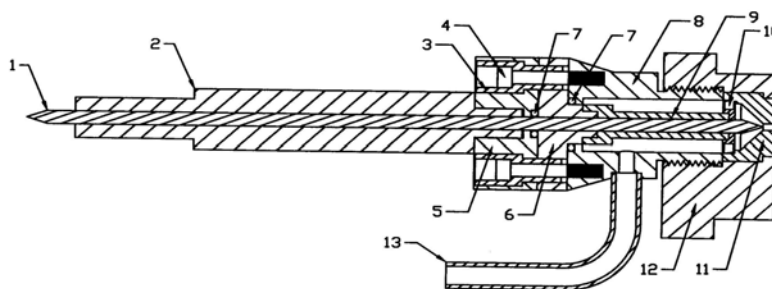
Figure A-5: Section drawing of plasma torch developed by Jacobsen [2001]

Gallimore and the author designed the most recent Virginia Tech plasma torch, show in Figure A-6. This torch was meant to be the smallest torch developed yet, and therefore the design had to be altered. This torch was designed for a series of experiments on the possibility of reducing drag using a plasma. The torch incorporated a

hollow cathode holder that held a small cathode tip. The hollow portion of the cathode holder was then used as the feedstock supply passage. The torch had a one-piece anode made from tungsten. This anode proved to be difficult to machine, but tungsten had to be used in order to achieve the desired lifetime for such a small anode. These torches have not been tested yet.
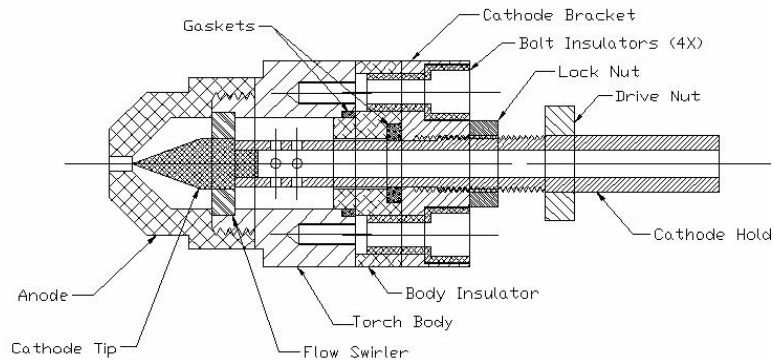
Figure A-6: Section drawing of the plasma torch developed by the author and Gallimore

The Virginia Tech Plasma Torch has improved greatly over the past twenty years. The torch has been made more reliable, and more compact. The development of the torch is summarized in Table A-1. The torch developed by Gallimore was used in the present work, and is described in detail in Chapter 3.

Table A-1 Virginia Tech plasma torches compared

Torch	Size (Diameter X length) [inches]	Improvement over Previous torch	Problems with Torch Design	Feedstocks used
Plasmadyne	2.5 X 2.5	-	Exit of torch not choked Designed for much higher powers than needed	Ar, H_2, Ar+ H_2
Barbi	1.5 X 3	Choked exit of torch	Electrode alignment difficult to achieve Short Electrode Lifetime	Ar, H_2, Ar+ H_2
Stouffer	1.75 X 4	Flow Swirler Longer electrode lifetime Improved electrode alignment	Difficult to change electrodes Overall size of the torch	Ar, H_2, Ar+ H_2, N_2, Air, CH_4, C_2H_6, C_3H_8
Gallimore	0.75 X 7	Reduced complexity Easier to change electrodes More compact design Reduced number of components		Ar, N_2, Air, CH_4, C_2H_6
Jacobsen	1.63 X 7	Anode Insert cheaper to manufacture Smaller body size	Anode inserts not as good for electrode alignment	Ar, N_2, Air, CH_4, C_2H_6
Gallimore and the author		Smaller size	Shorter electrode lifetime	Ar, N_2

Appendix B: Data Reduction Methods

This appendix documents the data reduction methods used to for the wind tunnel data taken in this study. Total temperature data reduction is discussed first. Next the triple rake data reduction methods is discussed. Finally, the spectrometer data reduction methods will be discussed

B.1 Total Temperature Data Reduction

The total temperature data was taken using a three-pronged total temperature rake. The rake traversed out into the flow during a run, moving spanwise in the test section between runs. The data from each probe was recorded as a column in the data file. These columns of data were extracted and reordered to arrange the columns by their spanwise location in the test section.

The total temperature data began when the traverse started moving, and ended when the traverse started to move back towards the floor of the wind tunnel. The traverse would stop and dwell at thirty stations on the way up. Thirty data points were taken at each station. The thermocouple would require some time before it settled at a steady value. Therefore only the last five data points were averaged to get the total temperature at that point.

The averaged total temperature was then divided by the averaged freestream total temperature at that time to get the total temperature ratio for that point. These total temperature ratios were then arranged and formatted for the plotting of line and contour plots.

B.2 Triple Probe Rake Data Reduction

In order to get a more detailed understanding of the flow downstream of the strut, a rake with a cone static, total pressure and total temperature probe was used. With this data, all of the important properties of the flow could be calculated. This data also had to be restructured by extracting the columns of data for all three probes at the same spanwise location. The data was then reduced for each station in the same way as for the total temperature data.

Once the data was reduced, the properties of the flow could be calculated. In order to calculate the properties of the flow, the flow regime had to be determined. Three different regimes were defined for this flow. The three regimes required three different methods for calculating the Mach number.

The first region was the upper supersonic region. In this region the curve fit equation shown in equation B-1 could be used. The upper supersonic region where this curve fit is valid is defined by a cone-static (Pcs) to measured total pressure (Po2) ratio of between 0.129 and 0.4782.

$$M = C_0 + C_1\sigma + C_2\sigma^2 + C_3\sigma^3 + C_4\sigma^4 + C_5\sigma^5 + C_6\sigma^6 + C_7\sigma^7 + C_8\sigma^8 + C_9\sigma^9 \quad \text{(B-1)}$$

$$\text{where } \sigma = 1.36942 - 2.86369\frac{P_c}{P_{02}}$$

and

$$C_0 = 1.19997, C_1 = 0.68905, C_2 = -0.13574, C_3 = 2.40341, C_4 = -4.04847, C_5 = 0.81891,$$
$$C_6 = 10.33433, C_7 = -16.45154, C_8 = 10.117, C_9 = -1.92393$$

Once the Mach number was known, the actual total pressure could be calculated from the measured total pressure and the Mach number using equation B-2. The difference in the actual and measured total pressure was due to the presence of the bow shock in front of the total pressure probe.

$$P_t = P_{t2}\left[\left[\frac{(\gamma+1)M^2}{(\gamma-1)M^2+2}\right]^{\frac{\gamma}{\gamma-1}}\left[\frac{\gamma+1}{2\gamma M^2-(\gamma-1)}\right]^{\frac{1}{\gamma-1}}\right]^{-1} \quad \text{(B-2)}$$

The local static pressure could then be calculated using equation B-3

90

$$P = P_t \left[1 + \frac{(\gamma - 1)}{2} M^2 \right]^{\frac{-\gamma}{\gamma - 1}} \qquad \text{(B-3)}$$

The recovery factor of the thermocouple probe was calculated using a few measurement points in the freestream. This calculated value was then used for the rest of the measurements. The recovery factor was calculated using equation B-3.

$$r = \left[1 + \frac{\gamma - 1}{2} M^2 \right] \frac{\left[\dfrac{T_t}{T_{t,\infty}} - 1 \right]}{\left[\dfrac{\gamma - 1}{2} M^2 \right]} \qquad \text{(B-4)}$$

The corrected total temperature could then be calculated using the recovery factor and the Mach number from equation B-5.

$$T_{t,corr} = T_t \left[\frac{1 + \dfrac{(\gamma - 1)}{2} M^2}{r \left(1 + \dfrac{(\gamma - 1)}{2} M^2 \right) - r + 1} \right] \qquad \text{(B-5)}$$

The static temperature could then be calculated using equation B-6

$$T = T_{t,corr} \left[1 + \frac{\gamma - 1}{2} M^2 \right]^{-1} \qquad \text{(B-6)}$$

The local mean velocity could be calculated from the Mach number and the static temperature using equation B-7.

$$u = M \sqrt{\gamma R T} \qquad \text{(B-7)}$$

Finally, the static density could be calculated using equation B-8

$$\rho = \frac{P}{RT} \qquad \text{(B-8)}$$

The second region of the flow was the lower supersonic region where the flow was still supersonic, but the curve fit equation was no longer valid because the shock was not attached to the cone-static probe. This region is defined by a cone-static probe measuring total pressure ratio of greater than 0.4782 and a Mach number greater than one. In this region equation B-2 had to be solved by assuming the static pressure was the same as the point above, a common assumption in boundary layer flows. Then equation B-2 could be solved simultaneously with equation B-3. Once the Mach number was known, the other properties of the flow could then be calculated as outlined above.

91

The final region was the subsonic region. In this region the static pressure was, again, assumed to be the same as for the point above. Also, in this region the measured total pressure was the actual total pressure, so there was no need to use equation B-2. The Mach number could then be calculated directly from equation B-3. Once the Mach number was known, all of the properties of the flow could then be calculated as outlined above.

B.3 Enthalpy Calculations

Once the properties of the flow were calculated as above, the enthalpy change of the flow could be easily calculated. The control volume for these calculations was assumed to be a rectangular volume with the free stream total temperature entering and the measured total temperature exiting. The energy addition of the plasma torch was not accounted for separately. The mass flow rate of air through an area of the grid was calculated using:

$$\dot{m} = \rho U (\Delta y \cdot \Delta z) \qquad \text{(B-9)}$$

Delta y was determined by the spanwise positions where measurements were taken. Delta z was determined by the difference in position between two vertical positions of the traverse.

The total enthalpy through a particular area of the grid was calculated using:

$$H_0 = \dot{m} \cdot C_{P,air} \cdot (T_{0,corr} - T_{0,\infty}) \qquad \text{(B-10)}$$

The constant pressure specific heat was assumed to be that of air. The free stream total temperature was taken at the same time as the total temperature at the measurement location. The total enthalpys of each area were then summed over the entire area to get the total enthalpy rise.

B.4 Uncertainty Analysis

Uncertainty play a large role in all experimental studies. Uncertainties come from two sources. The first is from systematic variations. These variations can be limited by regular calibration. All instruments used in this study were calibrated before any measurements were taken. The instruments were then checked regularly over the course of testing to ensure they remained in calibration.

The second source of uncertainty comes from the precision of all measurements. A analysis of this uncertainty was done for all the system used in the present study by Jacobsen [2001]. Jacobsen found the values found in Table B-1 for the uncertainty of the measurement systems used.

Table B-1: Estimated measurement uncertainties from Jacobsen [2001]

Quantity	Uncertainty
Total Pressure, P_0	± 0.04 atm
Static Pressure, P	± 0.001 atm
Static Temperature, T	± 4 K
Density, ρ	± 0.004 kg/m^3
Velocity, U	± 0.7m/s
Mach Number, M	± 0.03
Total Temperature, T_0	± 2 K
Enthalpy, H_0	± 11 W

These uncertainties account for normal operating error, but do not take into account special sources of error. Special sources of errors would be vertical or lateral probe positioning errors, probe misalignment with the flow, and run-to-run variation.

References

Barbi, E., "Uncooled Choked Plasma Torch for Ignition and Flameholding in Supersonic Combustion," Masters Thesis, Virginia Polytechnic Institute and State University, 1986.

Barbi, E., Mahan, J.R., O'Brien, W.F., and Wagner, T.C., "Operating Characteristics of a Hydrogen-Argon Plasma Torch for Supersonic Combustion Applications," Journal of Propulsion, Vol. 5, No. 2 (March-April 1989), pp. 129-133.

Brandstetter, A., Rocci, Denis, S., Kau, H. "Experimental Study on Transition between Ramjet and Scramjet Modes in a Dual-Mode Combustor," AIAA Paper 2003-7048, 12th AIAA International Space Planes and Hypersonic Systems and Technologies

Chen, D. C. C., Lawton, J., and Weinberg, F. J., "Augmenting Flames with Electric Discharges," *10th Symposium on Combustion*, Combustion Institute (1965), pp. 743-754.

Fujimori, T., Murayama, M., Sato, J., Kobayashi, H., and Niioka, T., "Flame-holding Behind a Wedge by Incident Shock Waves," *IUTAM Symposium on Combustion in Supersonic Flows*, (1997), pp. 95-110.

Gallimore, S. D., "Development and Operating Characteristics of an Improved Plasma Torch For Supersonic Combustion Applications," PhD Thesis, Virginia Polytechnic Institute & State University (May 2001).

Gallimore, S. D. "Operation of a High-Pressure Uncooled Plasma Torch with Hydrocarbon Feedstocks," Masters Thesis, Virginia Polytechnic Institute & State University (month year).

Gallimore, S. D., Jacobsen, L. S., O'Brien, W. F., and Schetz, J. A., "An Integrated Aeroramp-Injector/Plasma-Igniter for Hydrocarbon Fuels in Supersonic Flow, Part B: Experimental Studies of the Operating Conditions," AIAA 2001-1767, Presented at the 10th AIAA/NAL-NASDA-ISAS International Space Planes and Hypersonic Systems and Technologies Conference (April 2001).

Gallimore, S. D., Prebola, J. L., O'Brien, W. F., Schetz, J. A., Hanus, G., and Uznanski, K., "Operation of a High-Pressure Uncooled Plasma Torch on Hydrocarbon Feedstocks," Presented at the 36th JANNAF Combustion Meeting (October 1999).

Harrison, A. J., and Weinberg, F. J., "Flame Stabilization by Plasma Jets," *Proceeding of the Royal Society of London*, vol. 321, (1971), pp. 95-103.

Jacobsen, L. S., "An Integrated Aerodynamic-Ramp-Injector/ Plasma-Torch-Igniter for Supersonic Combustion Applications with Hydrocarbon Fuels," Ph. D Thesis, Virginia Polytechnic Institute & State University (April 2001).

Jacobsen, L. S., Gallimore, S. D., Schetz, J. A., O'Brien, W. F., and Goss, L. P., "An Integrated Aeroramp-Injector/Plasma-Igniter for Hydrocarbon Fuels in Supersonic Flow, Part A: Experimental Studies of the Geometric Configuration," AIAA 2001-1767, Presented at the 10th AIAA/NAL-NASDA-ISAS International Space Planes and Hypersonic Systems and Technologies Conference (April 2001).

Kimura, I., Hiroshi, A., and Manabu, K., "The use of a Plasma Jet for Flame Stabilization and Promotion of Combustion in Supersonic Airflows," *Combustion and Flame*, vol. 42, no. 3, (1981), pp. 217-305.

Lawton, J., Payne, K. G., and Weinberg, F. J., "Flame Arc Combination," *Nature*, vol. 193, no. 4817, (February 24, 1962), pp. 736-738.

Marconi, F., Bowersox, R., Orr, M., Mozingo, J., and Schetz, J., "Boom Alleviation Using Keel Configurations," AIAA Paper 2002-0149, AIAA 40th Aerospace Sciences Meeting and Exhibit, Reno, NV, Jan 14-17, 2002

Masuya, G., Chinzei, N. and Miki, Y., "Scramjet Engine Tests at Mach 4 and 6," IUTAM Symposium on Combustion in Supersonic Flows, (1995), pp. 147-162.

Masuya, G. et al., "Some Governing Parameters of Plasma Torch Igniter/ Flameholder in a Scramjet Combustor," *Journal of Propulsion and Power*, vol. 9, no. 2, (March-April 1993), pp. 176-181.

Northam, G. B., McClinton, C. R., Wagner, T. C., and O'Brien, W. F., "Development and Evaluation of a Plasma Jet Flameholder for Scramjets," AIAA 84-1408, Presented at the 20th Annual AIAA/ SAE/ ASME Joint Propulsion Conference, (June 1984).

Orrin, J. E., Vince, I. M., and Weinberg, F. J., "A Study of Plasma Jet Ignition Mechanisms," *18th International Combustion Symposium,* The Combustion Institute (1981) pp. 1755-1765

Sato, Y. and others, "Effectiveness of Plasma Torches for Ignition and Flameholding in Scramjet," *Journal of Propulsion and Power*, vol. 8, no 4, (July 1992), pp. 883-889

Stouffer, Scott, "Development and Operating Characteristics of an Improved Plasma Torch For Supersonic Combustion Applications," Masters Thesis, Virginia Polytechnic Institute & State University (July 1989).

Takita, K., Takatori, F., and Masuya, G., "Effect of Plasma Torch Feedstock on Ignition Characteristics in a Supersonic Flow," AIAA 2000-3586, Presented at the 36th Annual AIAA/ ASME / ASEE Joint Propulsion Conference, (July 2000).

Wagner, T. C., "Ignition and Flameholding in Supersonic Flow by Injection of Dissociated Hydrogen," Ph. D Dissertation, Virginia Polytechnic Institute & State University (February 1987).

Wagner, T. C., O'Brien, W. F., Northam, G. B., and Eggers, J. M., "Plasma Torch Igniter for Scramjets," *Journal of Propulsion and Power*, vol. 5, no 5, (September-October 1989), pp. 548-554

Warris, A. M., and Weinberg, F. E., "Ignition and Flame Stabilization by Plasma Jets in Fast Gas Streams," *20th International Symposium on Combustion*, The combustion Institute, (1984), pp. 1825-1831

Weinberg, F. J., "Old Flames and New," *Inaugural Lectures, Imperial College*, London (1968)

Vita

Joseph Alexander Mozingo was born in Rock Hill, South Carolina on March 17, 1977. He grew up in Edgemoor, SC. He attended Lewisville High School, and graduated in 1995. Joe then went to Clemson University, where he graduated with a Bachelor of Science degree in Mechanical Engineering in 2000. Joe currently lives in Rock Hill, South Carolina with his wife, Lauren, and dog, Rex.